LAWRENCE
LIVERMORE
NATIONAL
LABORATORY

LLNL-JRNL-401196

A Detailed Chemical Kinetic Reaction Mechanism for n-Alkane Hydrocarbons From n-Octane to n-Hexadecane

C. K. Westbrook, W. J. Pitz, O. Herbinet, H. J. Curran, E. J. Silke

February 11, 2008

Combustion and Flame

Disclaimer

This document was prepared as an account of work sponsored by an agency of the United States government. Neither the United States government nor Lawrence Livermore National Security, LLC, nor any of their employees makes any warranty, expressed or implied, or assumes any legal liability or responsibility for the accuracy, completeness, or usefulness of any information, apparatus, product, or process disclosed, or represents that its use would not infringe privately owned rights. Reference herein to any specific commercial product, process, or service by trade name, trademark, manufacturer, or otherwise does not necessarily constitute or imply its endorsement, recommendation, or favoring by the United States government or Lawrence Livermore National Security, LLC. The views and opinions of authors expressed herein do not necessarily state or reflect those of the United States government or Lawrence Livermore National Security, LLC, and shall not be used for advertising or product endorsement purposes.

A Detailed Chemical Kinetic Reaction Mechanism For n-Alkane Hydrocarbons From n-Octane to n-Hexadecane

By

Charles K. Westbrook, William J. Pitz
Olivier Herbinet[#], Henry J. Curran*, and Emma J. Silke
Lawrence Livermore National Laboratory
Livermore, CA 94550 USA

[#]now at ENSIC/INPL
Nancy, France

*now at University College of Ireland
Galway, Ireland

Abstract

Detailed chemical kinetic reaction mechanisms have been developed to describe the pyrolysis and oxidation of nine n-alkanes larger than n-heptane, including n-octane (n-C_8H_{18}), n-nonane (n-C_9H_{20}), n-decane (n-$C_{10}H_{22}$), n-undecane (n-$C_{11}H_{24}$), n-dodecane (n-$C_{12}H_{26}$), n-tridecane (n-$C_{13}H_{28}$), n-tetradecane (n-$C_{14}H_{30}$), n-pentadecane (n-$C_{15}H_{32}$), and n-hexadecane (n-$C_{16}H_{34}$). These mechanisms include both high temperature and low temperature reaction pathways. The mechanisms are based on our previous mechanisms for the primary reference fuels n-heptane and iso-octane, using the reaction class mechanism construction first developed for n-heptane. Individual reaction class rules are as simple as possible in order to focus on the parallelism between all of the n-alkane fuels included in the mechanisms, and these mechanisms will be refined further in the future to incorporate greater levels of accuracy and predictive capability. These mechanisms are validated through extensive comparisons between computed and experimental data from a wide variety of different sources. In addition, numerical experiments are carried out to examine features of n-alkane combustion in which the detailed mechanisms can be used to compare reactivities of different n-alkane fuels. The mechanisms for all of these n-alkanes are presented as a single detailed mechanism, which can be edited to produce efficient mechanisms for any of the n-alkanes included, and the entire mechanism, with supporting thermochemical and transport data, together with an explanatory glossary explaining notations and structural details, will be available for download from our web page.

INTRODUCTION

Practical fuels for transportation and other system fuels consist of complex mixtures of many types of hydrocarbon and related chemical species. Jet fuels, diesel fuel, gasoline and natural gas contain hundreds and often thousands of distinct chemical compounds. While not every chemical species contained in a practical fuel has been studied independently, these species can be collected into structural classes in order to understand the combustion properties and construct surrogate mixtures for those practical fuels. Recent studies have shown that it is productive to represent these practical fuels in terms of several basic structural classes of compounds, such as n-alkanes, branched or iso-alkanes, aromatics, polycyclic alkanes, olefins, naphthenes, and oxygenated hydrocarbons for gasoline [1], diesel fuel [2], and jet fuel [3,4]. Straight-chain or n-alkanes species are important components in all of these practical transportation fuels.

The structure of a hydrocarbon fuel has a profound impact on the ignition and other properties of that fuel. Empirical correlations between species molecular size and structure and ignition properties have existed for many years [5], based on experimental studies, and in recent years, the role of fundamental kinetic properties of these hydrocarbon fuels on ignition rates have become clearer [6-8]. Straight-chain hydrocarbons are more easily ignited under engine conditions than branched-chain hydrocarbons, and these ignition properties are commonly quantified in terms of octane number for spark-ignition engines and cetane number for diesel engines. Ignition properties are also of central importance in homogeneous charge, compression ignition (HCCI) engines and other configurations of similar behavior that involve low temperature combustion (LTC).

The familiar octane and cetane scales are both defined in terms of reference fuels which provide practical limits to ignition properties. For both scales, there is a fuel that defines very easy or early ignition and another fuel that defines late or difficult ignition. The fuel that defines zero octane number or easy ignition in spark-ignition engines is n-heptane, and the fuel that defines 100 cetane number or easy ignition in diesel engines is n-hexadecane, so in both cases, the reference fuel that is easily ignited is an n-alkane. The fuel that defines poor ignition for both scales is a highly branched hydrocarbon, iso-octane for gasoline and 2,2,4,4,6,8,8-heptamethyl nonane for diesel.

The easily ignited fuels, n-heptane and n-hexadecane, are noteworthy for the extensive amounts of low temperature kinetic reactions that they produce, reaction pathways controlled by alkylperoxy radical isomerization, and low temperature reactivity is an essential part of their rapid, early ignition kinetics. The highly branched fuels that define the low-reactivity limits of the octane and cetane scales are much slower to react because they exhibit little or no low temperature reactivity.

While the practical reference fuels are n-heptane and n-hexadecane, all of the n-alkane fuels from n-heptane to n-hexadecane and even larger are present in most practical transportation fuels. The present work focuses on the obvious structural similarities among these highly reactive n-alkane species, building on them to simplify the process of mechanism construction. This family of n-alkane fuels makes it possible to study the effects of fuel molecule size on combustion properties, while all of the fuels have the same general molecular structure.

We have had some success modeling both laboratory-scale experiments and practical engine phenomena with our past n-heptane kinetic mechanism [9], and the

present paper extends the same methodology to C_8 - C_{16} n-alkanes. Most important, the work of Curran et al. [9,10] defined kinetic mechanisms for large hydrocarbons in terms of specific reaction classes and exploited a modular form for mechanism construction that we have again employed in the present work. This type of construction has been used by others (e.g., [11-13]) and makes it quite simple to improve different reaction class descriptions as guided by new kinetics research.

The present reaction mechanisms are an attempt to provide "comprehensive" kinetic mechanisms, which use a wide variety of experimental inputs to validate the mechanisms [14,15]. This involves use of experimental results from shock tube, flow reactor, rapid compression machine, static reactor, stirred reactor, laminar flame, opposed flow diffusion flame, engine, and any other types of experiments to test the reaction mechanism. Comprehensive mechanisms for many fuels have been developed [9,10,16-24], largely for hydrocarbon molecules for which many types of experiments have provided validation data. Unfortunately, for the large n-alkanes of interest in this paper, there are fewer such experimental studies that provide good validation results. The present work includes as many as possible of such validation data, but they are rather sparse and limited in range.

Comprehensive chemical kinetic reaction mechanisms, such as those reported here, are inherently "works in progress" which are updated continuously, and this is certainly the case for these n-alkane fuels. As described below, we are aware of specific details in each mechanism in which improvements are possible. At the same time, the past success of the base n-heptane mechanism, as well as the overall good success of

these new mechanisms at reproducing the limited variety of experimental results available as described below, suggest that they can be useful in their current form.

The present combined n-alkane model is new in the sense of simultaneously providing a powerful chemical kinetic tool for an important range of practical hydrocarbon fuels, all with the same structural type, from n-heptane to n-hexadecane. However, kinetic mechanisms have been developed by other authors for some of the fuels included in the present mechanism.

An early detailed kinetic mechanism was developed in 1992 for n-hexadecane by Chevalier et al. [25], which included both high and low temperature reaction pathways and was used to simulate engine knock phenomena. This mechanism was already quite large, with approximately 1200 species and 7000 elementary reactions, and it was generated by a LISP language that specified rules for rates of various reaction types. A recent study [26] has recently demonstrated the capability to generate detailed kinetic mechanisms for alkane fuels of any desired size and illustrated this by analyzing experimental data for n-hexadecane.

The EXGAS code system developed at the DCPR/CNRS in Nancy [27-37] also has the capability of producing reaction mechanisms using established reaction rate rules, and it has been used to generate kinetic mechanisms for n-decane and n-hexadecane, and many others, addressing both high and low temperature oxidation regimes. Recent extensions in EXGAS capabilities have addressed cycloalkanes and cycloalkenes [32,33] and large alkenes [34-36] and used in analyses of HCCI combustion [37].

The group of Cathonnet and Dagaut at Orleans has also developed a large variety of kinetic mechanisms including those for n-decane and n-hexadecane [38-43]. Most of

these mechanisms were tested initially through comparisons between model calculations and experimental results, primarily from the Orleans jet-stirred reactor (JSR), which were carried out primarily within the high temperature regime.

Dagaut et al. [40,41] initially used n-decane as a surrogate to represent kinetics of kerosene for jet engine simulations. More recently, their work [42,43] has focused on using n-decane together with other surrogate compounds, especially cycloalkanes and aromatics, to better represent the soot production and emissions properties of kerosene. Dagaut et al. [44,45] recently extended this same approach to use a kinetic mechanism for n-hexadecane to simulate oxidation of rapeseed oil methyl ester.

Nehse et al. [46] developed detailed kinetic reaction mechanisms for n-decane and n-heptane to simulate intermediate temperature shock tube experiments for both fuels. Olchanski and Burcat [47] developed a reduced high temperature kinetic mechanism for n-decane to examine reflected shock wave ignition delay experiments. Bikas and Peters [13] developed a full temperature range kinetic mechanism to carry out n-decane combustion simulations is laminar flames, jet-stirred reactors, and shock tubes. Zhao et al. [48,49] developed a skeletal kinetic mechanism for high and intermediate temperature n-decane oxidation which, due to its skeletal construction based on partial equilibrium among alkyl radicals as developed in earlier studies of n-heptane [50], has the ability to carry out very efficient simulations under the experimental conditions for which it was developed. Recent kinetic modeling of pyrolysis in n-dodecane by Herbinet et al. [51] and Dahm et al. [52] have used the EXGAS approach to provide kinetic mechanisms to study pyrolysis of n-dodecane. Lindstedt and Maurice [53,54] developed n-heptane and n-decane reaction mechanisms and applied them to combustion of jet fuels.

A number of reviews of n-alkane combustion have appeared recently, each of which surveys kinetic modeling approaches as well as the relevant literature of experimental studies that can be used for model validation. Dagaut and Cathonnet [55] summarized a large body of experiments and kinetic modeling of kerosene combustion, showing how surrogate fuel mixtures including their n-decane kinetic mechanism can predict sooting behavior as well as overall heat release.

Buda et al. [56] discussed the importance of unified kinetic mechanisms for alkanes over both the low and high temperature regimes, an approach similar to that which has motivated the present work. Similarly, Ranzi et al. [57] used a "lumped" mechanism development approach to provide mechanisms for n-decane, n-dodecane and n-hexadecane. With the Ranzi techniques, mechanism lumping reduces the size of each mechanism and makes the resulting simulations reasonably efficient. Finally, Battin-Leclerc [58] has carried out a very recent review of low temperature experiments and kinetic models, intercomparing existing kinetic models for this regime.

In the current work, a family of chemical kinetic reaction mechanisms for large n-alkane fuels is developed for a variety of applications. Because of its modularity, it is quite simple to discard those portions that relate to n-alkanes larger than the fuel which is targeted for study. Similarly, the set of mechanisms are ordered logically so that the submechanisms relevant to low-temperature problems can be eliminated to provide a smaller, high temperature mechanism for applications such as flame propagation and some classes of high temperature shock tube, flow reactor, and stirred reactor applications. The different n-alkane mechanisms have a self-consistent kinetic approach, so that the differences in their predictions are due only to the different sizes of the fuels,

not to different submodels or assumptions made in parts of each mechanism. Future modifications can be made simultaneously for all the n-alkanes, with the goal being to keep the kinetic approach as similar as possible from one n-alkane to all the others. These mechanisms are validated in this paper as thoroughly as possible, given that relatively few kinetic studies have been reported for many of these larger n-alkanes. In some cases, the same experiments are simulated for each of the $C_7 - C_{16}$ mechanisms, leading to some interesting insights to hydrocarbon ignition that have not been previously appreciated.

KINETIC MECHANISMS

Basic Assumptions

Few experimental kinetic studies have addressed site-specific reaction rates or product pathways for fuels with 8 or more carbon atoms, including those in the present study. In addition, chemical reaction rate theory becomes expensive in computational terms as the number of heavy atoms exceeds 5 or 6. As a result, it is necessary to employ rules of similarity for the rates and products of the very large number of reactions in these models as described below. In cases where transition-state theory [59,60] or other theoretical approaches can provide better rate expressions, it is straightforward to replace the present approximate expressions with improved versions. Fortunately, sensitivity analyses suggest that in many cases, the specific reaction rate expression for any given elementary reaction can be less important than its product distribution.

We have used the THERM software [61] to compute thermochemical data for the species involved in the $C_8 - C_{16}$ n-alkane kinetic mechanisms. This provides an internally consistent set of values for specific heats, heats of formation, enthalpies of

formation and bond strengths that then produce consistent equilibrium constants and reverse reaction rates. There are other excellent alternative sources for thermochemical data (e.g., Yu et al. [62]) that can also be used. The modular mechanism construction of the present mechanism make it straightforward to exchange one set of thermochemistry for another as desired. We have chosen to restrict our focus to homogeneous kinetic problems and not address laminar flame problems, in order to assess the validity of the reaction mechanisms to problems that are purely kinetic in nature.

We use the reaction classes of Curran et al. [9,10] to present the details of the current mechanisms, and in most cases those reaction classes are retained intact, except as noted in the next section.

Following our previous practice, we will provide all of the new reaction mechanisms on our Web page at:

http://www-cmls.llnl.gov/?url=science_and_technology-chemistry-combustion

together with the required thermochemical tables. They are presented in Chemkin-compatible format, based on the widespread usage of that format. Again, the modularity of the mechanism presentation simplifies mechanism conversion to alternative formats. They are listed as one full mechanism, in a modular format to expedite editing to produce submechanisms as desired for specific n-alkanes smaller than C_{16}. In addition to simplified elimination of families of species and reactions larger than required for particular applications, the present format also makes it straightforward to remove species and reactions relevant to low-temperature oxidation applications

We expect to refine the present mechanisms continuously in the future. Among these anticipated upgrades are (1) a more general treatment of O_2QOOH isomerization reactions to include alternative reaction pathways, (2) implementation of the direct molecular elimination reaction path for production of olefin + HO_2 from decomposition reactions of alkylperoxy radicals, (3) three-parameter reaction rate expressions for addition reactions of alkyl + O_2 and QOOH + O_2 reactions, and (4) increased detail in reaction submechanisms for oxidation of large olefin species, including site-specific H atom abstraction reactions. The web-based mechanism files will be updated as these major mechanism improvements are made, along with documentation of the upgrades, although the earlier versions will also continue to be available. Changes will be intended to improve the theoretical underpinnings for the mechanisms and may not be required for many productive uses of the current mechanisms, as illustrated by the validation studies below. Almost any mechanism refinement will increase the size and complexity of that mechanism, making it more costly to carry out detailed kinetics simulations.

Notation

The specific details of the notation are summarized online as part of the mechanism documentation, but the simplest terms are described here for completeness. For a given n-alkane, we number the C atoms from one end of the linear chain, employing the reflection symmetry of this type of chain. Therefore, we can write:

$$\begin{array}{ccccccccccccccccccc} & & 1 & & 2 & & 3 & & 4 & & & & 4 & & 3 & & 2 & & 1 & & \\ 1 & - & C & - & C & - & C & - & C & & ..... & & C & - & C & - & C & - & C & - & 1 \\ & & 1 & & 2 & & 3 & & 4 & & & & 4 & & 3 & & 2 & & 1 & & \end{array} \qquad (1)$$

showing the first 4 C atoms at each end of an n-alkane chain. The numbers in Eq. (1) indicate H atoms in this n-alkane as well as the numbering of the H atom sites corresponding to the number of the C atom to which they are bonded. We number the C atoms as shown as the '1' site, the '2' site and continuing to the midpoint of the chain, then using the reflection symmetry to also number the sites from the opposite end of the chain. For n-hexadecane, the two middle C atoms would have the index '8'; for n-pentadecane there is only one '8' carbon atom, while for n-tetradecane there are two '7' C atoms and for n-tridecane there is only one '7' C atom. In the mechanisms, n-alkanes are named 'nc10h22' for n-dodecane, and similarly for the other n-alkanes.

There are therefore 3 H atoms attached at primary bonding sites at each end of these n-alkanes and indicated as '1' H atoms, with a total of 6 '1' H atoms in each n-alkane molecule. All of the other H atoms are bonded at secondary sites. The unique numbering of these secondary H atoms is intended to show that all of the '2' H atoms (of which there are four in the above diagram) are structurally identical and different from all the other sites, all of the '3' sites are also structurally identical and unique from all the other sites, and similarly for the remaining H atoms. The uniqueness of each of these sites leads to unique reaction product distributions to H atom abstraction and subsequent reactions. This is a key feature of a truly detailed, as opposed to a lumped or reduced reaction mechanism. These distinctions add a great deal to the complexity and size of a detailed reaction mechanism, but they also provide greater detail that may or may not justify the additional complexity, depending on the level of detail required. This type of detailed mechanism can subsequently be reduced by lumping together selected families

of structurely similar species with overall reaction rates, and the existence of the more fully detailed mechanism can then be very helpful in testing the capabilities of the reduced mechanism.

Alkyl radicals are indicated based on the H atom that has been removed from the chain above. Thus the c9h19-3 species indicates the result of abstracting a '3' H atom from n-nonane, while c16h33-7 represents the alkyl radical produced by abstracting a '7' H atom from n-c16h34. Subsequent addition of molecular oxygen to the c9h19-3 alkyl radical is shown by 'c9h19o2-3' , the related alkoxy radical is 'c9h19o-3' and the related hydroperoxide is 'c9h19o2h-3'.

Reaction Classes

Each of these reaction classes have been discussed in some detail in the mechanism descriptions for n-heptane [9] and iso-octane [10]. The "rules" for each of the reaction classes were not all the same in these two past studies, reflecting 4 years of mechanism development between the two mechanisms. For the current n-alkane mechanisms, we have emphasized the reaction class rules used for n-heptane, which are somewhat simpler than those for iso-octane and provide the most transparent and obviously parallel possible set of reaction rate rules for the present larger n-alkane fuels.

Detailed chemical kinetic reaction mechanisms are inherently works in progress. They are continually refined as new theoretical and experimental information appears, so the present work is a snapshot in time of a family of mechanisms. In every mechanism, the desired task is to optimize the description of available experimental results. This obligation to reproduce available data using imperfect mechanisms almost always results

in compensating errors in reaction pathways and reaction rate expressions in those mechanisms. When one part of a detailed mechanism is upgraded to reflect new data or kinetic understanding, other parts of that older mechanism must therefore also be changed, parts which had compensated for the errors being corrected in the new mechanism. The present mechanisms accurately reproduce a sufficiently broad range of available experimental results for large n-alkane combustion that they can be useful in many further studies and used to produce reduced and skeletal reaction mechanisms for efficient and accurate CFD simulations.

An overall reaction path diagram for hydrocarbon combustion and ignition in particular is shown in Figure 1.

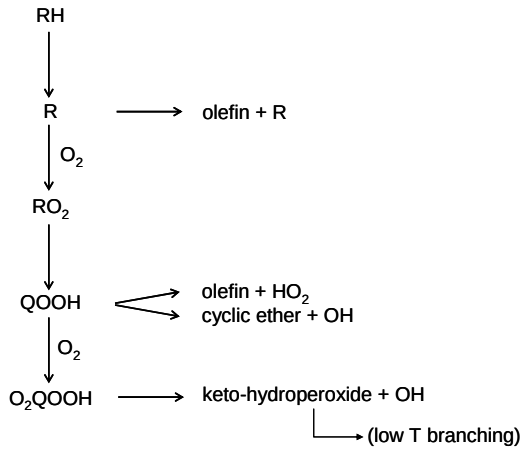

Fig. 1. Overall reaction path diagram describing hydrocarbon ignition at high and low temperatures.

HIGH TEMPERATURE MECHANISMS

Reaction Class 1: Unimolecular fuel decomposition

These reactions produce two alkyl radicals or one alkyl radical and an H atom. They provide chain initiation and, as the size of the hydrocarbon fuel increases, significant fuel consumption as well. Due to their high activation energies, the reactions producing H atoms are usually important only in the recombination direction, where they serve as sinks for H atoms. We prescribe these reaction rates in the exothermic or recombination direction, using the same rules and temperature-independent rates as in our previous n-heptane mechanism [9], and the rates in the decomposition direction are determined from microscopic reversibility and the thermochemistry of the individual species. For alkyl+H reactions, we assume a rate of 1 x $10^{14}$$cm^3$ mol^{-1} s^{-1}; when the recombination reactants include a methyl radical, we use a rate of 1.x10^{13} cm^3 mol^{-1} s^{-1} , and when both recombination reactants are larger alkyl radicals, we assume a rate of 8x10^{12} cm^3mol^{-1} s^{-1}.

Reaction Class 2: H-atom abstractions

These reaction rates depend on the abstracting radical, on the type of C - H bond that is being broken, which for these fuels are primary and secondary C - H bonds, and on the number of H atoms at equivalent sites. These values are very similar to those in our past mechanisms [9,10]. There are no tertiary C - H bonds in the n-alkane fuels discussed in the present work.

Reaction Class 3: Alkyl radical decomposition

Alkyl radical decomposition is important at temperatures above about 850K; below this temperature, alkyl radical addition to molecular oxygen is the major pathway

for alkyl radical consumption [63]. Because alkyl radical decomposition via β-scission is endothermic, we calculate the rate constant in the reverse, exothermic direction that is the addition of an alkyl radical (or H atom) across the double bond of an alkene, then computing the forward, β-scission rate constant from thermochemistry.

Reaction rate expressions for the reactions are very similar to those used in past reaction mechanisms for n-heptane and iso-octane. Rate constants for the addition of radicals across a double bond depend on (1) the site of addition (i.e., a terminal or internal C atom), and (2) the type of radical being added. Based largely on the work of Allara and Shaw [64], we assume that addition of an H atom across a double bond has a pre-exponential A-factor of 1 x 10^{13} cm^3 mol^{-1} s^{-1} with an activation energy of 1200 cal/mol if the H atom adds to the terminal C atom of the alkene, and with 2900 cal/mol if the H atom adds to an internal C atom. The rate constant for the addition of an alkyl radical has a lower A-factor and higher activation energy than for the addition of an H atom. We assume an A-factor of 1 x 10^{11} cm^3 mol^{-1} s^{-1} and an activation energy of 8200 cal/mol. We assume all these reactions are at their high pressure limit.

Reaction Class 4: Alkyl radical + O_2 = olefin + HO_2

This reaction class was discussed previously [9] , with a number of reasons why this direct reaction pathway was not included in our earlier reaction mechanism. A number of recent studies [65-68] have concluded that a direct, molecular elimination reaction of RO_2 can produce an olefin + HO_2 without proceeding via a QOOH intermediate and should be included in low temperature kinetic mechanisms. Most of the relevant research has focused on small hydrocarbon species such as ethyl and propyl

radicals, but it is likely that the same reactions occur for radicals as large as those in the present mechanisms. The present mechanisms do not include a direct reaction of R + O_2 to produce an olefin + HO_2, but they include sufficient detail in the reaction pathways available to the large alkyl radicals to describe n-alkane oxidation adequately.

Recent kinetic modeling studies, including n-heptane [9], cyclohexane [69] and methyl cyclohexane [70], have shown that a key to reproducing the overall rate of oxidation and the correct amount of negative temperature coefficient (NTC) behavior is to have an accurate description of the relative rates of chain branching, chain propagation, and chain termination in the reactions of the alkyl radicals from the fuel. Direct elimination reaction of alkylperoxy radicals is a propagation reaction pathway, producing an olefin and HO_2, so if this reaction class is added to the overall n-alkane mechanisms, then one or more corresponding changes would be needed to restore the proper balance of propagation with branching reaction paths. Either existing propagation reaction rates involving alkyl radicals would have to be reduced to compensate for the additional chain propagation, or rates of chain branching pathways would have to be increased correspondingly. This process was implemented for cyclohexane oxidation [69] and may be important in reproducing the pressure dependence of NTC behavior.

Reaction Class 5: Alkyl radical isomerization

These reactions transfer H atoms from one site in the radical to another via internal abstraction steps. Reaction rates depend on the type (i.e., primary, secondary or tertiary) of C - H bond being broken, on the ring strain energy of the transition state ring

involved, and on the number of equivalent H atoms available. The overall activation energy E_a is estimated using the expression

$E_a = \Delta H_{rxn} + \text{ring strain} + E_{abst}$

where ΔH_{rxn} is the enthalpy of reaction if the reaction is endothermic and zero otherwise. The activation energy for reaction is determined [71] from an Evans-Polanyi plot of E_{abst} vs ΔH_{rxn} (taken in the exothermic direction) of similar H atom abstraction reactions, leading to the following expression:

$E_{abst} = 12.7 + (\Delta H_{rxn} \times 0.37)$

The A factors were obtained using RADICALC [72], a computer code that implements transition state theory and calculates the change in entropy of the radical to the transition state due to loss or gain of internal rotors and optical isomers.

At temperatures close to 1000K, these isomerization processes are quite rapid, creating an effective equilibrium among all the alkyl radicals. The rates of alkyl β-scission have higher activation energies than the energy barriers for isomerization, so under such conditions the decomposition of alkyl radicals takes place from an equilibrium pool of alkyl radicals. Dryer et al. [48-50] have exploited this feature in reaction mechanisms for a number of n-alkane fuels to reduce the mechanisms significantly for more efficient computations, at little or no loss of generality. However, this process can be done only for temperatures where isomerization is rapid and β-scission is slow.

Reaction Class 6: H atom abstraction from olefins

Very few detailed kinetic mechanisms are available for any large olefin species, including those considered in the present n-alkane mechanisms. Battin-Leclerc [58] has surveyed the entire literature and found no olefins larger than pentene or hexene with kinetic reaction mechanisms that distinguish between olefin isomers and provide site-specific reaction rates for elementary reactions. Recent attention on kinetic experiments and modeling has focused on pentenes and hexenes [32,34-36,73], and new work, not yet published, by Mehl et al. [74] has developed a kinetic mechanism for the isomers of hexene and used that mechanism to study RCM experiments of Vanhove et al. [73], but overall this is an area in which a great deal more kinetic research is needed.

To oxidize olefins produced in these n-alkane mechanisms, we have estimated rates for H atom abstraction reactions from olefin species. Abstracting radicals are limited to H, OH, O, and CH_3 radicals and products are lumped into a single alkenyl radical for each n-alkane fuel. Thus there is only one $C_{10}H_{19}$ radical in the n-decane mechanism, and one $C_{16}H_{31}$ alkenyl radical in the n-hexadecane mechanism. This is an over-simplification and more work is needed. If the fuel consists of an n-alkane fuel, sensitivity analyses indicate that the present treatment of the olefins and alkenyl radicals is satisfactory, but when the fuel is a large olefin, this simplification is not suitable.

Reaction Class 7: Addition of radical species to olefins

This reaction type is treated in the same manner as in past mechanisms for n-heptane and iso-octane. Addition reactions of olefins with H atoms and CH_3 radicals are already included as the reverse direction of β-scission reactions in Reaction Class 3. Addition reactions of HO_2 radicals are also included as described below for Reaction

Class 20. The remaining radical additions of O and OH are treated as composite reactions, with addition of the O or OH radical to either side of the olefin double bond. In our treatment, the resulting oxygenated adduct is not treated as a separate species but is assumed to decompose via a β-scission type of reaction. In the present mechanisms, we have attempted to identify the most likely product distributions for these decompositions and include the overall reaction as an "elementary" reaction. Like several other features of these n-alkane reaction mechanisms, this approach is satisfactory when the primary fuel under examination is an alkane, but when the primary fuel is an olefin, this treatment must be refined further to include a more detailed description.

Reaction Class 8: Alkenyl radical decomposition

The present n-alkane mechanisms include a somewhat improved treatment of the decomposition of the lumped alkenyl radicals, as compared with the prior treatment of our n-heptane and iso-octane mechanisms [9,10]. While there is only a single alkenyl radical for each n-alkane fuel, the alkenyl radical is now assumed to decompose to a wide range of smaller products, with each decomposition reaction producing a smaller olefin and alkenyl species. In the absence of a much more careful kinetic modeling of n-olefins and their products, this lumping of alkenyl radicals and the detailed variety of their decomposition reactions is a temporary but effective solution, with some similarities to the alkyl lumping used by Dryer et al. [48-50]. These unimolecular decomposition reactions are assigned a rate expression of $1.0 \times 10^{13} \exp(-45000/RT)\ s^{-1}$.

Reaction Class 9: Olefin decomposition

In some model computations, large olefin species decompose at appreciable rates. For all of the present mechanisms, we have used the same rate constant expression of $1x10^{16}$ exp(-71000/RT) s-1. In previous large molecule mechanisms, we used an A-factor of 2.5×10^{16}, but in the present mechanisms, we have included a larger variety of product pathways for each olefin and reduced each A-factor to give approximately the same overall rate of olefin decomposition. This is a very simplified treatment of a complex set of reactions, and more research is needed to refine this subject area.

LOW TEMPERATURE MECHANISM

The following reaction classes are commonly identified as "low temperature" reaction pathways, which is somewhat oversimplified. The key overall process is Reaction Class 10, the addition of an alkyl radical to molecular oxygen and the equilibrium constant of such addition reactions. If this equilibrium strongly prefers the adduct RO_2, then the "low temperature" reaction sequences will contribute to the rate of combustion, and if the equilibrium strongly favors the dissociation to $R + O_2$, then only the Reaction Classes 1 - 9 are generally required. The transition from high to low temperature regimes is not sharply defined, and increasing pressure can extend the "low temperature" regime to higher temperatures. Much of the present low temperature kinetic mechanism is based on the work of Pollard [75].

Reaction Class 10: Alkyl radical addition to O_2

Rates of addition reactions of radical species to O_2 were assumed to depend primarily on the type (primary, secondary, or tertiary) of alkyl radical to which the O_2 is added. For the present n-alkane mechanisms, we have selected a single addition rate and decomposition rate for each of the two types of alkyl radicals in these n-alkane fuels. These rates are based on microscopic reversability and are approximately correct. This simplified treatment will provide a good basis for mechanism comparisons, and future improvements will provide better descriptions of variations of the equilibrium of these reactions with temperature and pressure.

In the present mechanisms, for primary alkyl radicals, the R + O_2 addition reactions all have the same rate expression of 4.52 x 10^{12} cm^3 mol^{-1} s^{-1} and decomposition rate expressions of 2.66 x 10^{20} $T^{-1.67}$ exp(-35400/RT) s^{-1}. For secondary alkyl radicals, all of the addition reactions have the rate expression of 7.54 x 10^{12} cm^3 mol^{-1} s^{-1} and decomposition rate expression of 1.36 x 10^{23} $T^{-2.36}$ exp(-37670/RT) s^{-1} .

Reaction Class 11: R + R'O_2 = RO + R'O

Reactions of alkyl radicals with alkylperoxy radicals are estimated to occur at 7.0 x 10^{12} exp(+1000/RT) cm3 mol^{-1} s^{-1}, as assumed in our previous iso-octane mechanism and close to the rate used in our n-heptane mechanism. The reverse rates are based on microscopic reversibility. We include only those reactions in which the R and R' alkyl radicals have the same number of carbon atoms. That is, for the n-dodecane mechanism, we include such reactions as $C_{12}H_{25}$-2 + $C_{12}H_{25}O_2$-5 = $C_{12}H_{25}O$-2 + $C_{12}H_{25}O$-5, but we do not include $C_{12}H_{25}$-2 + $C_{11}H_{23}O_2$-5 = $C_{12}H_{25}O$-2 + $C_{11}H_{23}O$-5. The reasoning for this choice is that we expect the R and R'O_2 levels to be significant only for the R and R'O_2 corresponding to the carbon number of the initial fuel, with the rates of all "cross reactions" with R and R' with different numbers of carbon atoms being negligibly slow because either the R or R' would be orders of magnitude smaller than the other.
We also include reactions of the form R + HO_2 = RO + OH, using the same rate expression of 7.0 x 10^{12} exp(+1000/RT) cm^3 mol^{-1} s^{-1}, used above. This group of reactions had not been included in either the n-heptane or iso-octane mechanisms and were included here for completeness.

Reaction Class 12: Alkylperoxy radical isomerization

These reactions provide the key reactions for low temperature hydrocarbon oxidation pathways. The sources of these reaction rates, including those used here, have been discussed previously [10]. These reactions proceed via internal transfer of H atoms, initially bonded to C atoms in the alkane chain, to the terminal O atom in the alkyl peroxy radical site. The transition state rings which facilitate these reactions have 5, 6, 7, and 8 atoms, and the elementary rates vary with the size of that transition state ring (i.e., ring-strain energy barrier), and the type of C - H bond that is broken to transfer the H atom. The importance of these reactions is that the 5-, 7- and 8-membered transition state rings primarily produce chain propagation, while only the 6-membered transition state rings produce significant amounts of chain branching. The product distributions of low temperature oxidation also are different for each transition state ring size, and this information is needed to calibrate all of the reaction rate parameters for this class of reactions.

Reaction Class 13: $RO_2 + HO_2 = ROOH + O_2$

This reaction class uses a rate expression of 1.75×10^{10} exp(+3275/RT) cm^3 mol^{-1} s^{-1}, and the reverse reaction rate is computed using microscopic reversibility. This reaction is relatively unimportant because other reactions of RO_2 are usually much faster than this bimolecular reaction.

Reaction Class 14: $RO_2 + H_2O_2 = ROOH + HO_2$

This reaction rate expression is the same as that for previous mechanisms, 2.4 x 10^{12} exp(-10000/RT) cm^3 mol^{-1} s^{-1}, based on Tsang's recommendation [76] for the reaction $CH_3O_2 + H_2O_2 = CH_3O_2H + HO_2$. This reaction is isoergic, and the reverse reaction is assumed to have the same rate as the forward reaction.

Reaction Class 15: $RO_2 + CH_3O_2 = RO + CH_3O + O_2$

The only reaction of this type that has been studied in detail is $CH_3O_2 + CH_3O_2 = CH_3O + CH_3O + O_2$. We estimated the rate of this reaction in our iso-octane mechanism to be 1.40 x 10^{16} $T^{-1.61}$ exp(-1860/RT) cm^3 mol^{-1} s^{-1}, and this rate expression is used in the present mechanisms. We assume that the termolecular reverse reaction has a zero rate.

Reaction Class 16: $RO_2 + R'O_2 = RO + R'O + O_2$

The rate expressions for this class are assumed to be the same as those above for the similar Class 15. As in Class 11, we assume the rates of these reactions are significant only when R = R', that is, when both R and R' have the same number of carbon atoms.

Reaction Class 17: $RO_2H = RO + OH$

In early combustion kinetics analyses, this reaction was believed to be extremely important, following the abstraction of H atoms from the fuel and other stable

hydrocarbons by RO_2 radicals. At lower temperatures, formation and decomposition of RO_2H would provide degenerate branching and contribute significantly to the onset of ignition. The greater importance of RO_2 isomerization reaction pathways has become recognized, and current kinetic modeling produces relatively minor levels of RO_2H. Decomposition of alkyl hydroperoxides can still be very important in situations where they are added to sensitize a reactive mixture.

In the present mechanisms, we use a rate expression 1.5×10^{16} exp(-42500/RT) $cm^3\ mol^{-1}\ s^{-1}$ when R is a primary radical and 1.25×10^{16} exp(-41600/RT) $cm^3\ mol^{-1}\ s^{-1}$ when R is a secondary radical, reflecting the slightly different bond strengths of the O-O bonds, similar to recommendations of Sahetchian et al. [77] for 1-heptyl and 2-heptyl hydroperoxides. The rate of the reverse reaction, in the recombination direction, is determined using microscopic reversibility.

Reaction Class 18: Alkoxy radical decomposition

These decomposition reactions are assumed to proceed via formation of an aldehyde and an alkyl radical, an analogy with β-scission reactions of large alkyl radicals [63]. Like β-scission reactions, these reactions are written in the addition direction, with rate expressions of 1.0×10^{11} exp(-11900/RT) $cm^3\ mol^{-1}\ s^{-1}$ when R is a primary radical and 1.0×10^{11} exp(-12900/RT) $cm^3\ mol^{-1}\ s^{-1}$ when R is a secondary radical.

Reaction Class 19: QOOH decomposition and production of cyclic ethers

These reactions involve breaking the O-O bond in the QOOH radical, followed by the formation of a cyclic compound. The rates of these reactions are assumed to depend

primarily on the number of atoms in the cyclic portion of the molecule, or equivalently, to the ring strain energy barrier to forming the cyclic structure. The major uncertainty regarding these reaction rates is the way the A-factors are estimated. As the size of the transition state ring grows, there is a loss of entropy as internal rotors are eliminated, and the A factor of the reaction decreases. In the initial n-heptane mechanism [9], the A-factors decrease by factors of 12 with each increase in the number of atoms in the transition state ring, but this factor of 12 was changed to a factor of 8 for the iso-octane mechanism [10] to better match the distributions of the product cyclic ethers, and these factors of 8 are retained in the present mechanism.

Reaction Class 20: QOOH beta decomposition to produce olefin + HO_2

When the radical site in the QOOH radical is on the C atom adjacent to the COOH group, the radical can decompose to produce an alkene and HO_2. The rates of all of these reactions are assumed to be the same, at $1.61 \times 10^{20}\ T^{-2.52} \exp(-21350/RT)\ s^{-1}$ in the decomposition direction and $1.0 \times 10^{11} \exp(-11530/RT)\ cm^3\ mol^{-1}\ s^{-1}$ in the addition direction. In the addition direction, this reaction provides a pathway for reaction of HO_2 with olefin species.

This β-decomposition reaction of QOOH plays a significant role in determining the rate of low temperature ignition of hydrocarbons and the extent of NTC behavior. It represents a chain propagation route for RO_2 isomerizations, which compete with pathways that lead to chain branching. The balance between chain propagation and branching has been shown [69,70] to be the most important factor in reproducing the extent of NTC behavior. Recent studies [65-68] have indicated that a direct reaction of

RO_2 proceeds through a direct molecular elimination path to produce a conjugate olefin and HO_2, rather than via QOOH intermediates; such direct eliminations pathways provide additional chain propagation, which therefore requires either reduced propagation via alternatives such as QOOH = olefin + HO_2 or increased chain branching in other reactions, in order to maintain the balance needed to reproduce observed NTC behavior. Experimental evidence [78] suggests that this QOOH = olefin + HO_2 reaction may have a somewhat higher energy barrier than is used in the present mechanism, and recent modeling results for low temperature oxidation of cyclohexane [69] demonstrated that a direct molecular elimination pathway for R + O_2 can be combined with a reduced rate of QOOH = olefin + HO_2 to retain the observed NTC behavior by maintaining the ratio of propagation to branching. We expect to revisit all of the RO_2 reaction pathways as the present mechanisms are upgraded in the future. However, the current mechanisms do provide the proper balance between propagation and branching and can reproduce observed behavior in hydrocarbon ignition at low temperatures.

Reaction Class 21: QOOH decomposition to small olefin, aldehyde and OH

When the QOOH radical is produced from RO_2 via a six-membered transition state ring, the QOOH can then decompose via a β-scission reaction to produce a carbonyl product and an olefin, followed by an O-O bond scission that produces OH; the overall products thus consist of OH, an aldehyde and an olefin. In our previous n-heptane mechanism, we assigned these reactions a direct decomposition rate expression, but in the iso-octane mechanism we assumed a rate expression for the addition of the olefin and the carbonyl species of 1.0×10^{11} exp(-11900/RT) cm^3 mol^{-1} s^{-1} and then compute the β-

scission reaction from this expression and microscopic reversibility. We characterize this process in the mechanisms as an "elementary" reaction with three products and a zero reverse rate, discounting the possibility of the olefin, aldehyde and OH recombining to produce the QOOH original species. Since the olefin and aldehyde are relatively stable products, this reaction class is effectively a chain propagation pathway since it produces only one OH radical species.

Reaction Class 22: Addition of QOOH to molecular oxygen O_2

Addition reactions of QOOH with O_2 are the only pathways at low temperatures that provide significant chain branching via production of multiple radical species, as outlined below. The equilibria of these reactions are strongly temperature dependent, with decomposition reaction activation energies of about 36 kcal/mol and addition reaction activation energies of approximately zero, and these equilibria are ultimately responsible for NTC behavior in the oxidation of these n-alkanes.

We have assumed that the rates of these addition reactions are the same as the addition reactions of alkyl radicals with O_2 described above for reaction class 10, varying only from the type (i.e., primary or secondary) of site in the QOOH species at which the addition occurs. In principle, the dissociation reaction rate expression is computed from the forward rate via microscopic reversibility. However, in the present mechanism, we have set all of the dissociation reactions involving reactions at primary sites equal to a single, characteristic dissociation rate expression, and another representative rate expression for dissociation involving secondary sites. We consider that any systematic inaccuracies in this process are less than the uncertainties in forward reaction rate

expressions and the relevant equilibrium coefficients, but we expect to determine more specific dissociation reaction rate expressions in the future.

Reaction Class 23: O_2QOOH isomerization to carbonylhydroperoxide + OH

These reactions are quite complex, including an internal H atom abstraction via a cyclic transition state, followed by O-O bond breaking and then formation of a C=O carbonyl bond. Rate expressions for this class of reaction are the same as those for comparable RO_2 isomerization reactions in reaction class 12, except that the activation energies are reduced by 3 kcal/mol. This reduction is due to the fact that the H atom being abstracted is bound to a carbon atom with an attached hydroperoxy group, which lowers the C-H bond energy by approximately 3 kcal/mol. In addition, the A-factors from O_2QOOH isomerization reactions must be adjusted to reflect the lower number of H atoms available at the target site due to the presence of the OOH group.

This current treatment assumes that the internal H atom transfer process is limited to H atoms at sites in the O_2QOOH species where the original H atom abstraction occurred in the n-alkane molecule. The reasoning, noted just above, is that the OOH group at the site of the initial H atom abstraction makes the remaining H atoms easier to abstract and that they will be the predominant pathway for isomerizations. However, many of the remaining H atoms at other sites in the O_2QOOH species can also be abstracted in isomerization steps, at rates comparable to those included in the present formulation. We have included some of these "alternative" isomerization reaction pathways in previous mechanisms, particularly when the fuels are highly branched as in some isomers of heptane [7] or in fuels with limited numbers of conventional

isomerization pathways [69], but they are not yet included in the present n-alkane mechanisms. In the present case of n-alkanes, there are so many possible O_2QOOH isomerization pathways with relatively low activation energies that the inclusion of alternative pathways does not affect the rate of ignition to any significant degree, but future revisions of these mechanisms will add these reaction pathways.

Reaction Class 24: Carbonylhydroperoxide decomposition

Decomposition of these complex carbonylhydroperoxide species starts with breaking the O-O bond to produce OH, followed by a radical decomposition step that produces a carbonyl radical and a stable product, usually an aldehyde. Thus this reaction produces two radicals and an aldehyde, and the aldehyde is a fairly reactive type of stable species; the overall effect in the reaction mechanism is a considerable degree of chain branching.

We write this series of processes as a single reaction in the mechanism, in spite of the complexity of the multiple processes actually occurring. The rate for the "reaction" is estimated by recognizing that the first step involves breaking the O-O bond. Although the thermochemistry of each carbonylhydroperoxide species is different, we have assigned two rates for all of the possible decomposition reactions, one at $1.5 \times 10^{16} \exp(-42000/RT)\ s^{-1}$ for all of the decompositions where the OOH is located at a primary C site and $1.05 \times 10^{16} \exp(-41600/RT)\ s^{-1}$ for all of the decompositions where the OOH is located at a secondary C site, again based on recommendations of Sahetchian et al. [77] for decompositions of 1-heptyl and 2-heptyl hydroperoxides.

Reaction Class 25: Reactions of cyclic ethers with OH and HO_2

Cyclic ethers are produced at lower temperatures and consist of large hydrocarbons with oxygen atoms imbedded in the molecule. There is very little kinetic information, especially including site-specific reaction rates, that is available for this class of species. A cyclic ether produced from n-tetradecane would have the formula $C_{14}H_{28}O$ with a cyclic ring of 3, 4, 5, or 6 atoms, one of which is the O atom in the molecule. Thus there is also a chain of carbon and hydrogen atoms of considerable length, and there is a good probability that H atom abstraction would be the major feature of their consumption. Since these species are formed predominantly at low temperature, we have assumed that the most important H atom abstractions are reactions with OH and HO_2 radicals, which are the most significant radicals at lower temperatures. Abstraction reactions with H, O, CH_3 and other radicals can easily be included in a mechanism, especially if the large cyclic ethers were the primary fuels in a system. Since cyclic ethers from the large n-alkanes are produced only at low temperatures, reactions involving breaking C - C bonds are unlikely to be significant consumers of the cyclic ethers. Again, if these species were parts of the primary fuel and present in significant amounts, then additional consumption pathways should be included.

Core mechanism

The above detailed reaction mechanisms are built upon a core mechanism for the smaller C/H/O species. The core H_2/O_2 mechanism was taken from O'Conaire et al. [21]

and the C_1-C_4 submechanism for the present work was developed by Curran [79] and is itself a constantly-evolving submechanism which is included in the overall mechanism.

These are large reaction mechanisms which require significant amounts of computer disk space and memory to execute, and on some laptop computers with limited capacities, the largest of these mechanisms cannot be accommodated. The mechanism for n-hexadecane includes 8130 elementary reversible reactions among 2116 chemical species, and these totals increase when additional submechanisms are added, such as a reasonably complete NOx submode or a soot submodel.

The sizes of some of the fuel mechanisms from C_{10} through C_{16} when species and reactions for larger fuels have been removed are the following:

	$C_{16}H_{34}$	$C_{14}H_{30}$	$C_{12}H_{26}$	$C_{10}H_{22}$
Reactions	8130	6449	5030	3878
Species	2116	1668	1282	940

.

VALIDATION STUDIES

Unlike many smaller hydrocarbon fuels such as methane, propane or even n-heptane, the larger n-alkanes have received much less attention in kinetic studies, and relatively few studies have been published that can be used for mechanism validation. Fortunately, when the few available sources are combined from all of n-alkanes included in this mechanism development, they cover most or all of the parameter ranges that are commonly encountered. These include shock tube ignition, rapid compression machine ignition, jet stirred reactors, flow reactors, and laminar flames, covering both high temperature and lower temperature phenomena. The majority of these data have been obtained for n-decane combustion, with much smaller numbers of studies of the other n-alkanes. As shown below, we found it interesting to combine groups of experimental data analyses and computed results to examine a unified description of n-alkane ignition in the rapid compression machine and for intermediate and high temperature shock tube conditions.

High temperature shock tube ignition

High temperature shock tube ignition of larger n-alkanes has been studied by Olchanski and Burcat [47], Davidson et al. [80,81], and Zhukov et al. [82,83] for n-decane, and the present n-alkane mechanism was used to simulate their results. Larger hydrocarbons have rarely been studied in shock tube experiments, primarily because the low volatility of the liquid fuels makes it difficult to prepare homogeneous gas-phase fuel/oxidizer mixtures. For these calculations with n-decane fuel, the portions of the full

mechanism describing C_{11} - C_{16} kinetics were removed, making the calculations more efficient, as noted above.

Olchanski and Burcat [47] investigated the shock tube ignition delay of mixtures of n-decane and oxygen, diluted in argon. Eight distinct mixtures containing 0.49% to 1.5% n-decane and 4.16% to 23.25% O_2 were included, with temperatures ranging from 1239K to 1616K and pressures from 1.82 to 10 atm. A total of 144 shocks were analyzed, and their paper includes specific, representative results from 30 of them.

Computed results with the present mechanism are compared with the experiments in Figure 2. The results for the richest mixture 7 at $\phi = 3$ are not shown, for which all four shocks in that group showed relatively poor agreement, with the computed results igniting faster than the experiments by factors of approximately 10.

For the shocks shown in Fig. 2, the agreement between experimental and computed ignition delay times is mixed, with some shocks providing very good agreement and others with only fair agreement. In most cases, the computed ignitions are faster than in the experiments, with overall better agreement at lower temperatures than at the highest range of temperatures.

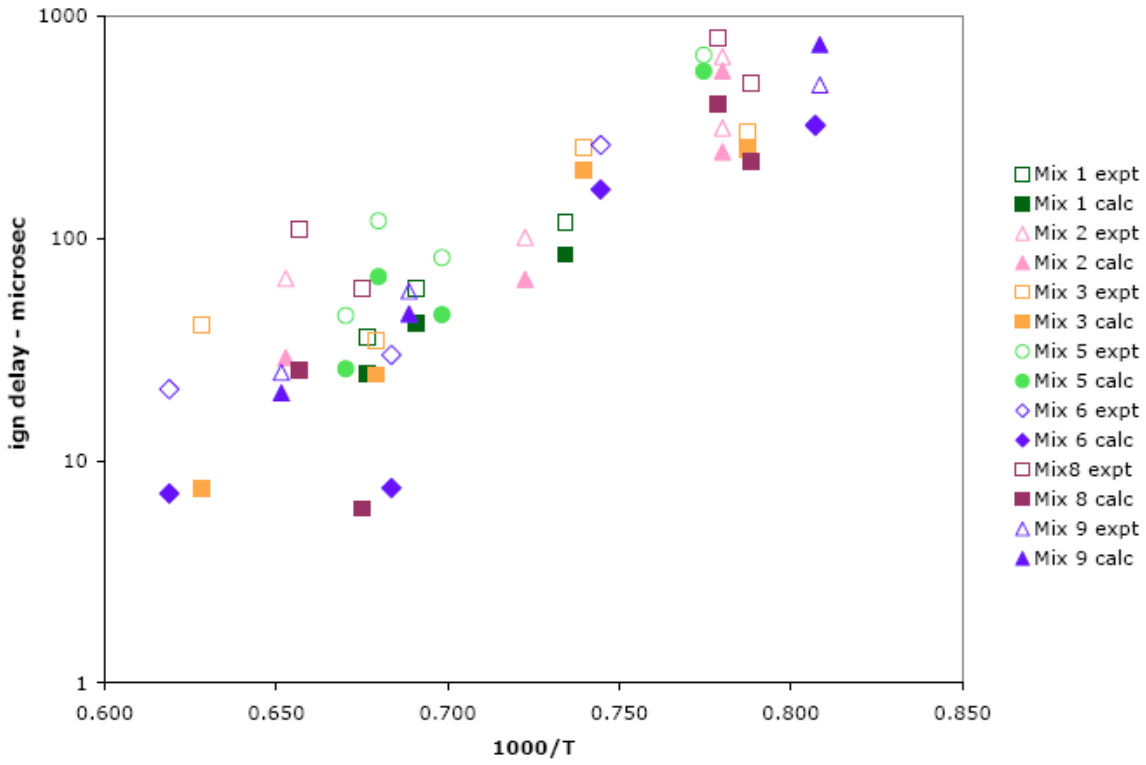

Fig. 2. Computed and experimental [47] ignition delay times for n-decane/O_2/Ar mixtures behind reflected shock waves. Experiments are shown as filled symbols, computed results as open symbols, so each shock is represented by a pair of symbols.

Frequently, reflected wave shock tube experiments of hydrocarbon ignition provide only ignition delay times for use in mechanism validation. Such integrated measurements are useful but often are of limited value. Some recent studies have added the capability of measuring selected radical concentrations during the ignition delay period, providing a much more demanding test of a reaction mechanism. Davidson et al. [80] measured OH concentrations during the shock tube ignition of n-decane.

These shock tube experiments were carried out at temperatures from 1400K to nearly 1800K, in the high temperature regime for the kinetic schemes. Post-shock pressures were all about 2 atm, and the reactive mixtures are all close to stoichiometric and very dilute in argon. Four groups of shocks were reported, three groups with 300

ppm n-decane at $\phi = 0.8$, $\phi = 1.0$ and $\phi = 1.2$, and a fourth, stoichiometric group with 2000 ppm n-decane. A representative example of the measurements is shown as the dashed curve in Figure 3, with a negligible induction period, followed by a fairly steep rise to a level of about 200 ppm at about 225 μs. The experimental results were characterized by the time at which the OH reaches half its maximum level, which is marked by the bar on the time axis at 154 ms. The second indicator is the final "plateau" level of the OH concentration, which is at 206 ppm, shown by the bar on the right hand side of the figure.

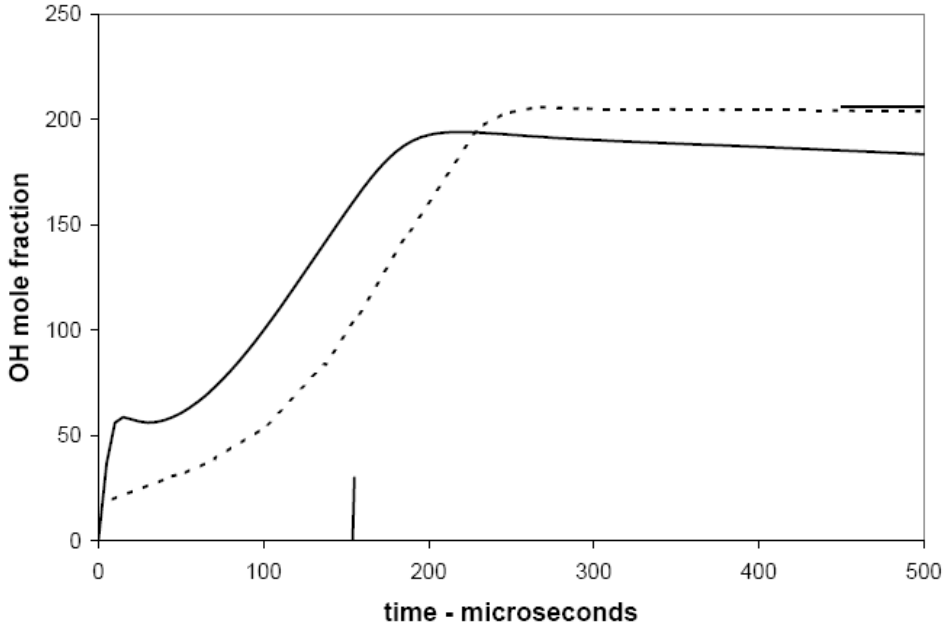

Fig. 3. Experimental [80] and computed OH mole fractions in n-decane ignition. To=1525K, $\phi = 1$, n-$C_{10}H_{22}$ initial concentration is 300 ppm.

The results of the model simulation are shown as the solid curve on Fig. 3, showing a slightly earlier rise in OH concentration followed by a rapid rise to a final level very similar to that measured experimentally. The computational OH curve reaches half ots

final value at about 100 ms, whereas the experimental value is 154 ms, and the experimental and computed plateau OH levels are nearly equal. Two additional examples of these results are shown in Figure 4, from two of the other groups of shocks.

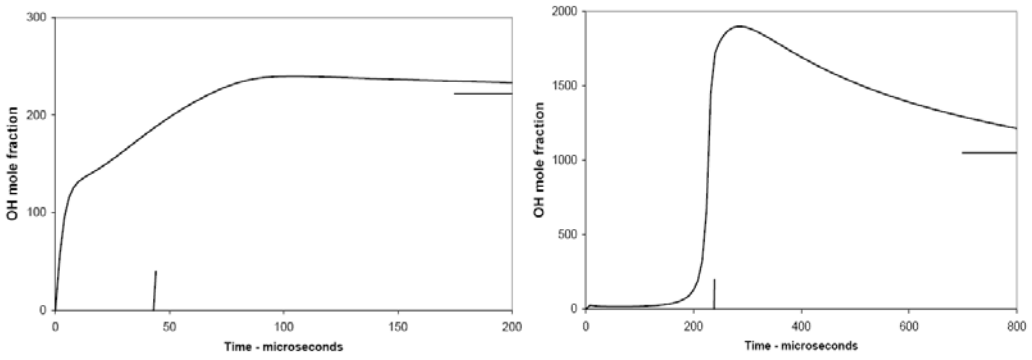

Fig. 4. Computed OH concentrations for (left) To=1706K, 300 ppm n-decane, $\phi = 1.2$, and (right) To=1404K, 2000 ppm, $\phi = 1.0$. Experiments from [80].

In the first case in Fig. 4, the model reproduces the midpoint of the rise in OH and the plateau value quite well. In the second case, the increased fuel content (i.e., 2000 ppm) produces enough energy to make the ignition very rapid, and the time of ignition is captured accurately by the model. In the same case, the OH overshoots its final value, and it is evident that the computed OH is falling towards its plateau value at a somewhat longer time scale than the end of the computation.

Intermediate temperature shock tube experiments

Intermediate temperature shock tube experiments have been carried out by Adomeit et al. for mixtures of n-heptane and air [84] and, more recently, n-decane and air [85]. The n-heptane/air experiments were carried out at 6.5, 13.5 and 40 bar pressure and for stoichiometric, lean and rich fuel/air mixtures. The experiments for n-heptane /air

have been widely used to validate fully detailed, as well as reduced or skeletal kinetic mechanisms for n-heptane oxidation. The n-decane experiments, at pressures of 13 bar for equivalence ratios of 0.5, 1.0 and 2.0, and at 50 bar for equivalence ratios of 0.67, 1.0 and 2.0, have also been used for the same purposes of validation of recent mechanisms for n-decane/air kinetics.

The experiments, as illustrated in Figure 5, show a transition from low temperature to high temperature ignition, with a negative temperature coefficient (NTC) region between them. The n-heptane experiments demonstrate not only the NTC behavior but also the variation in NTC behavior with equivalence ratio and with pressure. In particular, increasing pressure and increasing equivalence ratio moved the NTC region to gradually higher temperatures but also reduced the magnitude of the NTC behavior.

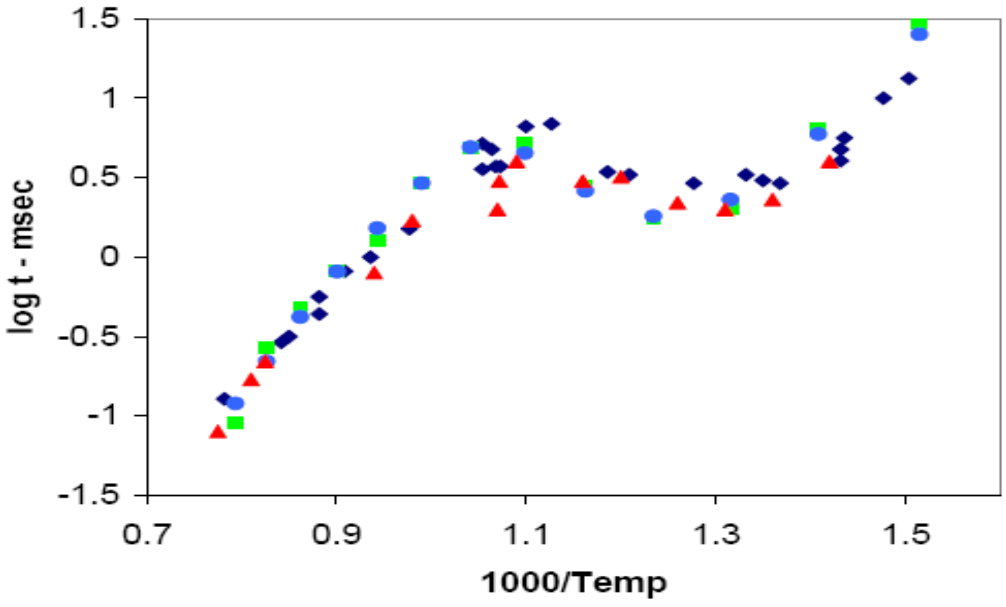

Fig. 5. Shock tube ignition delay times for n-heptane and n-decane, all at 13.5 bar pressure and stoichiometric fuel/air. Experiments are from (♦)Ciezki and Adomeit [84] and (▲) Pfahl et al. [85]. N-heptane (■) computed results from ref [9], n-decane (●) results computed from the current mechanism.

Nehse et al. [46] examined these ignition results for n-heptane and n-decane using a somewhat lumped kinetic mechanism, successfully reproducing the major features of the temperature and equivalence ratio variations for both fuels. Another interesting result of Nehse et al. was that the computed ignition delay times for stoichiometric n-decane/air at 13.5 bar pressure were nearly identical to the results for n-heptane/air. Pfahl et al. [85] noted similarities between the ignition delays of these fuels but noted that the n-decane results had slightly shorter ignition delays at lower temperatures. Pfahl et al. also noted that α-methyl naphthalene did not show the NTC behavior of the n-alkanes and that dimethyl ether showed more rapid ignition that the n-alkanes at low temperatures. Other modeling studies in the rapid compression machine [86] have also used the n-decane experimental results for model validation and will be discussed below.

The experimental results for both stoichiometric n-heptane and n-decane mixtures in air at 13.5 bar are compared with computed results using the present kinetic mechanisms are plotted in Figure 5, showing very good agreement for both fuels. Similar close agreement was found for mixtures at 6.5 and 40 bar pressures and at equivalence ratios of 0.5 and 2.0 for n-heptane/air and 0.67 and 2.0 for n-decane. The higher pressure experiments are of particular value for mechanism validation because they address pressures encountered during ignition in diesel and HCCI engines and under knocking conditions in spark-ignition engines. Computed results by Nehse et al. also showed excellent agreement with the same experimental results.

Although experimental results are available for comparison only for n-heptane and n-decane, we carried out a complete series of simulations at 13.5 bar initial pressure for each n-alkane from n-octane through n-hexadecane at stoichiometric conditions to

assess the ignition behavior of each n-alkane, and the results are shown in Figure 6. Within the uncertainties of the calculations, each fuel shows virtually identical ignition delay times except within the NTC region, where there is a slight but definite trend where the ignition delay time increases as the length of the n-alkane chain increases, with the most pronounced differences located at an initial temperature of about 810K.

This family of computed problems has some interesting features. For these n-alkanes, each mixture is stoichiometric in air. One n-octane molecule has only half the number of C atoms as n-hexadecane, with nearly the same ratio (18/34) of H atoms as well, so the amount of air required to consume a molecule of n-octane is only approximately half that required to consume a molecule of n-hexadecane. For each fuel, a stoichiometric mixture is nearly all air, with a very small amount of fuel. For example, the present n-octane/air mixture contains 98.35% air and only 1.65% n-octane, while the n-hexadecane/air mixture contains 99.15% air and 0.85% n-hexadecane. Initial compositions of the other stoichiometric n-alkane/air mixtures vary monotonically between these two limits and all are approximately 99% air and between 0.85% and 1.65% fuel. While they all contain nearly equal amounts of oxygen, there are twice as many n-octane molecules as n-hexadecane molecules in their respective stoichiometric fuel/air mixtures. The physical properties of all these mixtures are almost completely determined by the properties of air, but their chemical properties are controlled entirely by the kinetics of the different fuels. As our present example will show, these differences in initial compositions provide the key to explaining the behavior of these systems. As already noted, the only differences between the results in Fig. 6 are the cases for initial temperatures near 810K, so we have selected those results at 810K for further analysis.

The computed temperatures for each n-alkane, initially at 810K, are shown in Figure 7, showing a two-stage ignition with each fuel. The first stage ignitions begin at very nearly the same time and end at nearly the same temperature for each fuel, and the computations indicate that this "plateau" temperature is determined from the equilibrium of the R + O_2 = RO_2 reactions. Since all of these fuels are dominated by secondary C - H bonds, this similarity in plateau temperature is not surprising. The onset of the second, final stage ignition stage increases monotonically with the length of the n-alkane chain. This is surprising, since the cetane number of these alkanes increases from n-octane to

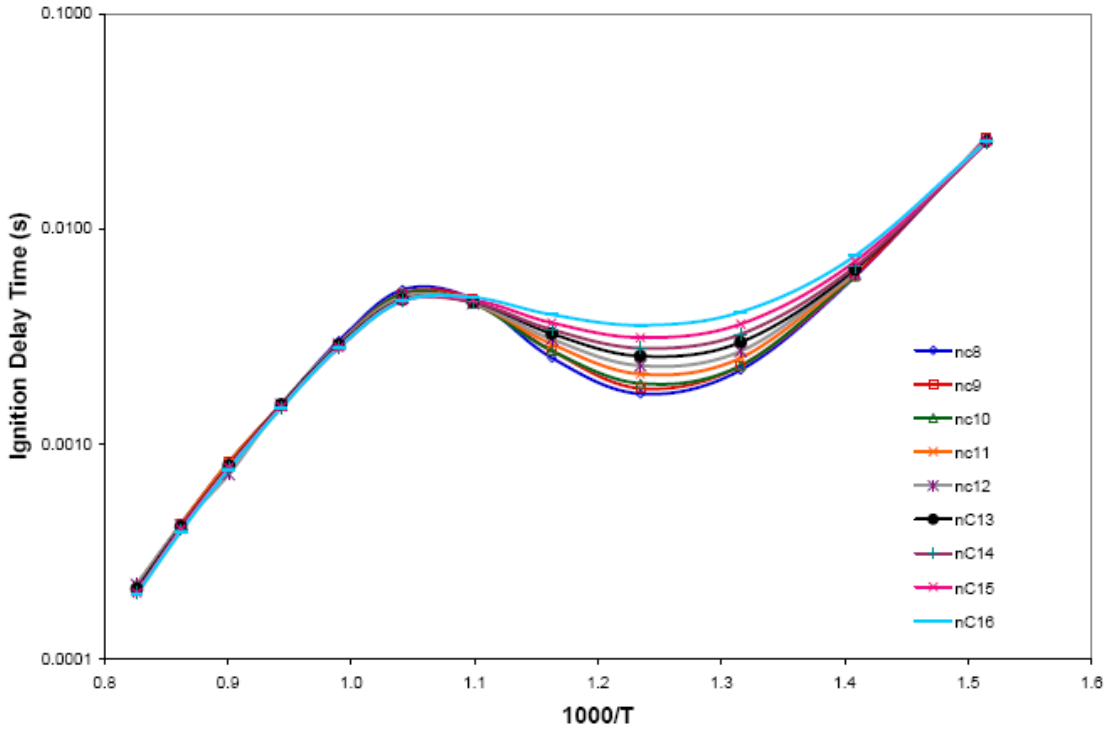

Fig. 6. Computed ignition delay times for stoichiometric n-alkanes in air at 13.5 bar.

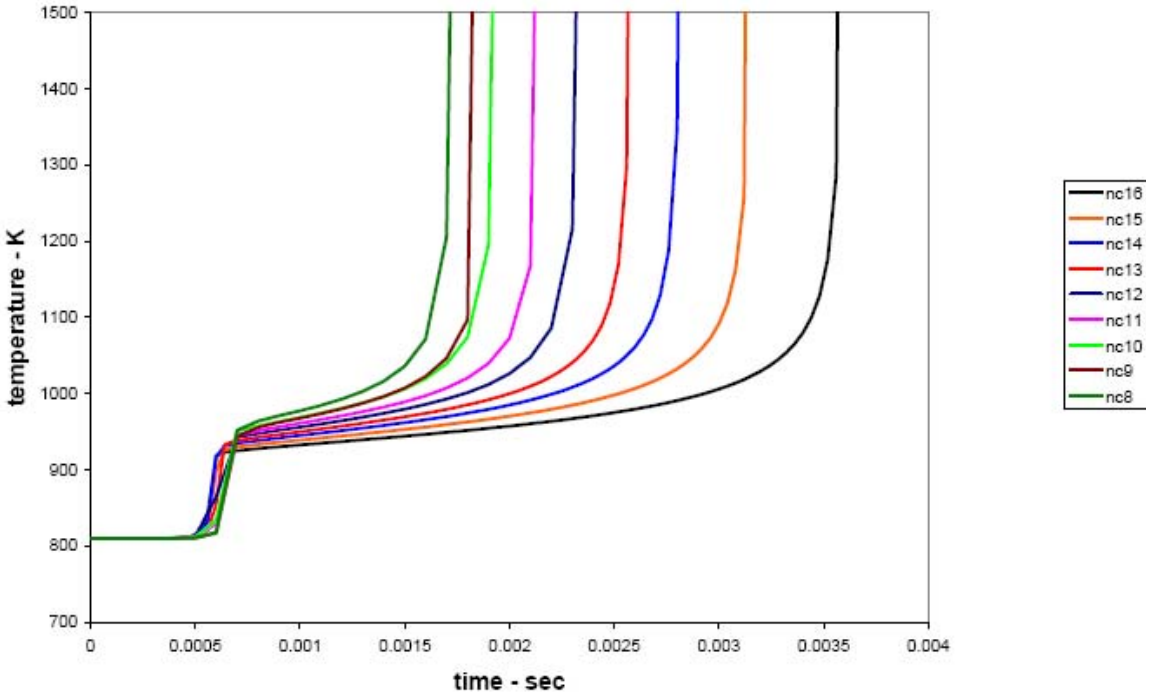

Fig. 7. Computed temperatures during ignition of stoichiometric n-alkane/air mixtures from n-octane to n-hexadecane, showing two-stage ignitions. For each fuel, the initial temperatures are 810K and 13.5 bar pressure.

n-hexadecane, and since cetane number is viewed as an indication of the ignition quality or ignition timing of these fuels, it might appear that these fuels should ignite in the order of cetane number rather than the reverse order shown in Figs. 6 and 7. However, the ignition of diesel fuel that determines cetane ratings has been shown by Dec [87] to involve ignition at very fuel-rich conditions ($\phi \sim 3$-4), not at the stoichiometric conditions as those shown in Figs. 6 and 7. In addition, liquid fuel must vaporize and mix with air in diesel engine ignition, and the vaporization rates of these fuels vary more rapidly with n-alkane chain length than the kinetic ignition rates vary. Further ignition studies using the present mechanisms under relevant rich conditions are needed to address this question.

Closer examination of the temperature profiles in Fig. 7 show that, while very similar, the temperatures following the end of the first stage of the ignition show a systematic variation, with the n-octane level being highest (~957K) and n-hexadecane lowest (~927K), with a monotonic variation between these limits. While the differences are quite small, higher temperatures following the first stage correspond to fuels that eventually ignite earlier.

The n-alkane fuel mole fractions during ignition are plotted in Figure 8, showing very clearly that the fractional amount of fuel consumption during the first stage ignition is smallest for n-octane and largest for n-hexadecane. Specifically, the initial mole fraction of n-octane is 0.0165, and after the first stage, its mole fraction is 0.006, a reduction of 64%. The corresponding reduction in n-hexadecane is from an initial mole fraction of 0.0085 to a lower level of 0.0006, a reduction of 93%, and the reductions in levels of the other n-alkanes vary monotonically between these limits.

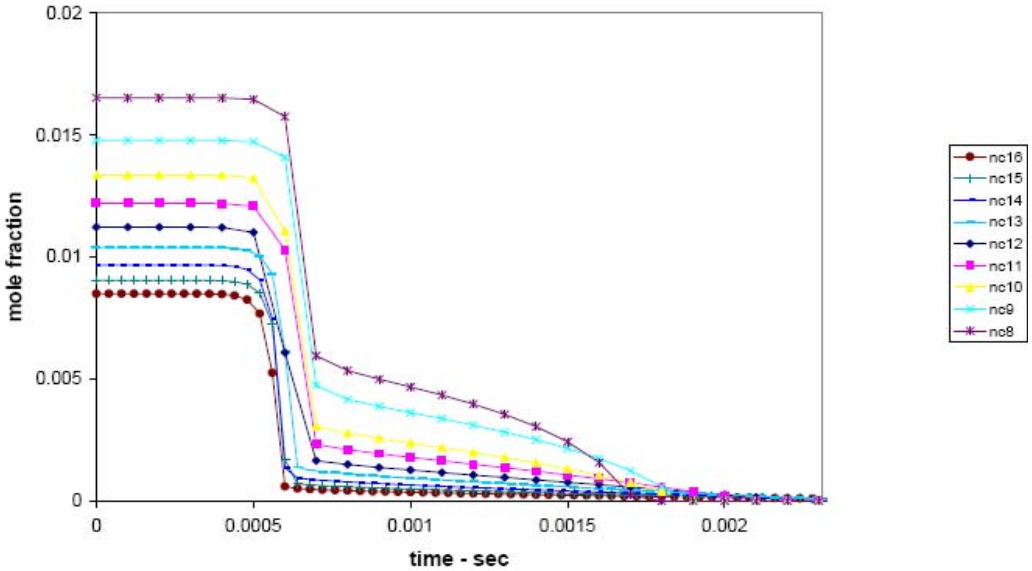

Fig. 8. Consumption of fuel during the first ignition stage for n-alkane fuels. Initial temperature in each case is 810K, 13.5 bar pressure, at stoichiometric conditions in air.

However, the absolute amounts of n-octane consumed during the first stage are much larger than the absolute amounts of n-hexadecane consumed. For n-octane, the reduction from its initial mole fraction of 0.0165 to 0.006 consumes 0.0105 mole fraction units of n-octane molecules, while only 0.0079 mole fraction units of n-hexadecane molecules are consumed, with the intermediate n-alkanes consuming intermediate amounts of n-alkane molecules. All these trends are results of the fact that these are stoichiometric mixtures of n-alkanes with air, and the initial n-octane concentration is twice that of n-hexadecane.

At the elevated pressures of these shock tube experiments (13.5 bar), the low temperature regime for hydrocarbon oxidation is at its peak of activity at 810K, the initial temperature for each calculation shown in Figs. 6-8. Under these conditions, the low temperature alkylperoxy radical isomerization reaction pathways are responsible for most of the chain branching that produces the first stage ignition. Each alkyl radical produces, at most, one low temperature reaction chain, regardless of the length of the carbon chain in the alkyl radical. As a result, since more n-octane molecules are consumed and more octyl radicals are produced overall from the larger amounts of n-octane fuel molecules than hexadecyl radicals when n-hexadecane is the fuel, there is more (i.e., nearly twice as much) low temperature reactivity for n-octane than for n-hexadecane and more heat is released, leading to the earlier ignition of the n-octane. Larger numbers of n-octane molecules in the fuel produce larger numbers of alkyl radicals, more chain branching, and more heat release via low temperature oxidation kinetics than in n-hexadecane oxidation under the stoichiometric conditions of these experiments and calculations. This trend is

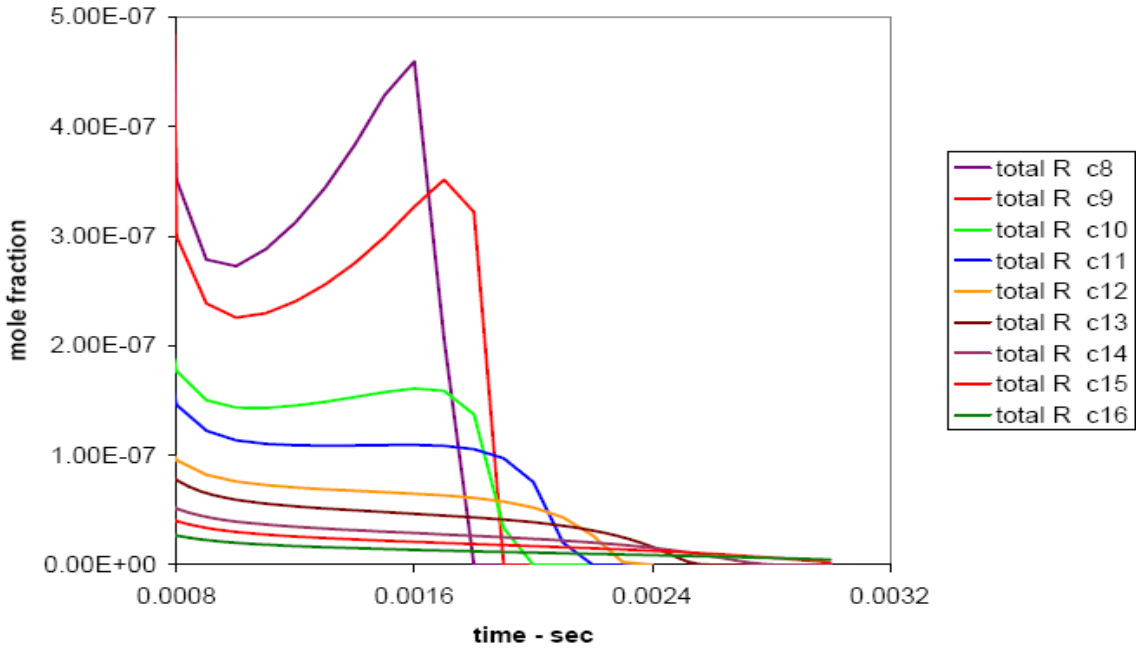

Figure 9. Computed total alkyl radical concentrations following first stage ignition for a series of n-alkanes.

illustrated clearly in Fig. 9, showing the total fuel alkyl radical levels for each fuel, at a time just following the end of the first ignition stage. For n-octane, n-nonane and n-decane, the total alkyl levels increase during the delay period leading up to the second stage ignition, while the alkyl levels for the larger n-alkanes remain almost constant. It is evident that higher alkyl populations lead to higher overall rates of reaction and an earlier second stage ignition.

Rapid compression machine experiments

The low and intermediate temperature regimes for hydrocarbon oxidation are often studied experimentally in the rapid compression machine (RCM). Typical reaction temperatures in RCM experiments are from about 650K and 900K, which spans the negative temperature coefficient (NTC) region which has important implications for

hydrocarbon ignition in internal combustion engines. Many laboratory groups have studied systems in the RCM, but RCM experiments have the same limitations of low vapor pressure as noted above for shock tube experiments. We could find only one study of ignition of n-alkanes larger than n-heptane; Kumar et al. recently carried out RCM experiments [86] specifically with n-decane. In the Kumar et al. experiments, vaporized mixtures of n-decane, oxygen and diluent are mixed at an equivalence ratio of 0.8. Low pressure gas mixture temperatures are varied in order to achieve a range of compressed temperatures, and these gases are then compressed rapidly to pressures in the range from 7-30 bar and temperatures of 630-706K. The experiments use a novel piston design to remove as much as possible of the boundary layer gases that form during the compression stroke and make the determination of the post-compression gas mixture temperature especially difficult. The post-compression ignition delay times were measured and compared with computed results using the reaction mechanism developed by Bikas and Peters [13]. The general trends in the experiments were reproduced qualitatively well by that mechanism, but the actual ignition delay times from the model were consistently longer than the corresponding experiments by factors of 4 - 5. For example, at a compressed mixture pressure of 30 bar and temperature of 662K, the measured ignition delay was 4.5 ms while the calculated ignition delay was about 22 ms. Kumar et al. do not address the reasons for the significant differences between their measurements and the modeling predictions, but use the term “over-prediction” when summarizing the computed values.

We repeated the ignition delay simulations using the present n-alkane mechanism, and a series of results over a range of compressed gas initial temperatures at 14.3 bar

pressure is shown in Figure 10. The results show a familiar pattern of two-stage ignitions for compressed gas temperatures of 680K to 740K. As observed by Kumar et al., these

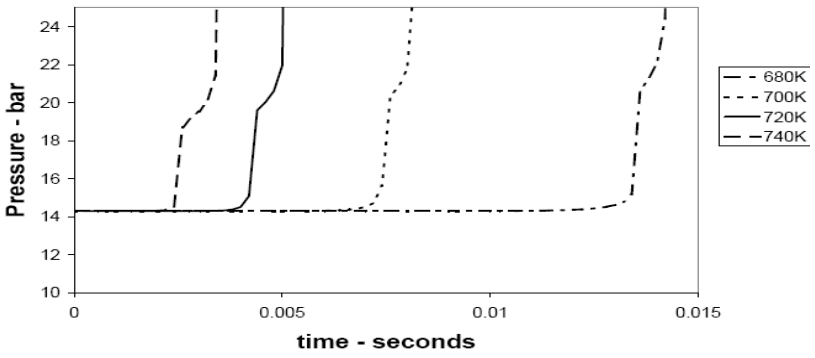

Fig. 10. Computed pressures in RCM experiments at 14.3 bar pressure, $\phi = 0.8$, with n-decane and air, at different compressed gas temperatures

computed results did not show any NTC behavior, which would be expected at temperatures higher than those represented in the experiments.

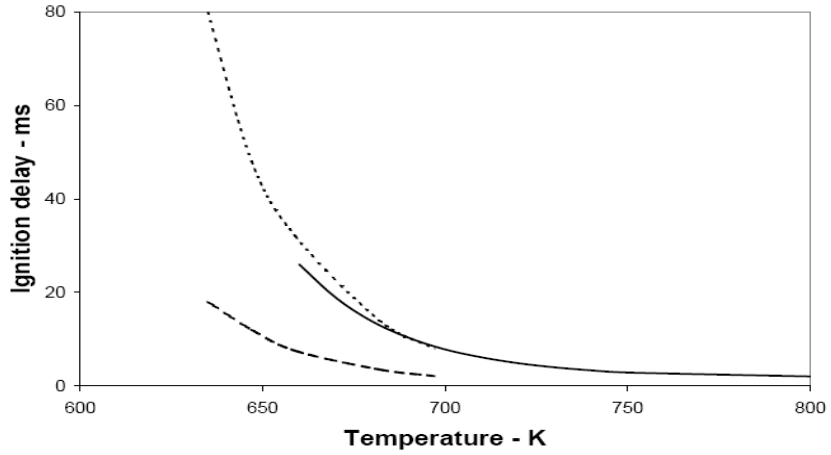

Fig. 11. Ignition delay times at different compressed gas temperatures for n-decane/air in the RCM at $\phi = 0.8$ and 14.3 bar pressure. Dashed curve, experiments [86], dotted curve, computed results [13], solid curve, present model.

Interestingly, our computed results are in generally better agreement with the computed results using the Bikas and Peters [13] mechanism for n-decane than they are with the experimental results. The three sets of results are summarized in Fig. 11.

Kumar et al. then adopted a very interesting approach for data analysis, combining their RCM experimental results with the intermediate temperature shock tube experiments for n-decane of Pfahl et al. [85] and Zhukov et al. [83]. The assumption is very common and well accepted that essentially no reaction occurs in the shock tube until the extremely rapid rise in temperature and pressure at the time of shock arrival, but the compression stroke in the RCM, achieving similar temperatures and pressures as in the shock tube, occurs over a longer period of time than in the shock tube. However, if no appreciable reaction occurs during the compression stroke, then it is logical to conclude that RCM and shock tube ignition delay times at the same temperature, pressure and equivalence ratio should be equal.

Exactly the same concept was used recently by Petersen, Curran et al. [88,89] when they intercompared shock tube and RCM ignition delay measurements for propane ignition. In the case of Petersen et al., the RCM data and several sets of shock tube results showed excellent agreement, but some shock tube studies showed results that were inconsistent from the rest, and on that basis, Petersen et al. went on to question the reliability of the inconsistent set of shock tube results.

Following the examples of Kumar et al. and Petersen, Curran et al., we have plotted together several sets of RCM and shock tube data for the ignition of n-decane/air at 13 - 14 bar initial pressure in Figure 12. The experimental RCM results of Kumar et al. and the computed results using the Bikas and Peters mechanism were obtained at an

equivalence ratio of 0.8, while the present model results and the shock tube results of Ciezki et al. [84] and Pfahl et al. [85] were obtained for stoichiometric mixtures. We scaled the results from $\phi = 0.8$ to 1.0 by a factor of 0.95, in order to compare with

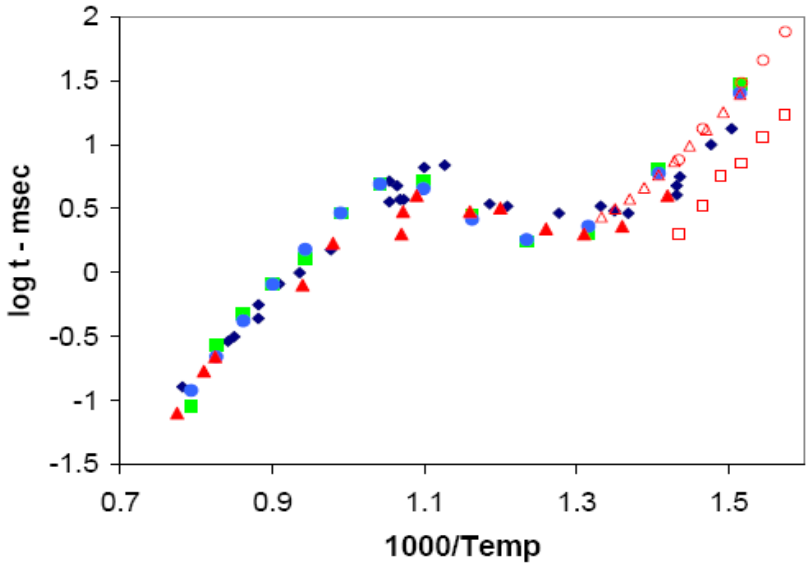

Fig. 12. Ignition delay times for stoichiometric n-decane in shock tubes and rapid compression machines at approximately 14 bar pressure. RCM data (□) of Kumar et al. [86] and RCM results computed by Bikas and Peters (○)are scaled from ϕ=0.8 for comparison, RCM results computed by present model (Δ). All other symbols for shock tube ignition are the same as in Fig. 5.

stoichiometric results, based on ratios of computed results. In addition to these n-decane results, stoichiometric experimental and computed shock tube ignition delay times at 13.5 bar pressure [84,85] are also included in Fig. 12 to provide additional calibration of the experimental and kinetic modeling results.

When the experimental results of Kumar et al. are compared with the computed and experimental results for the shock tube ignition of n-decane and n-heptane, it is clear from Fig. 12 that the results of Kumar et al. are slightly faster than all the other results. If we believe that the results should be internally consistent, then there must be some reason

for the faster ignition of n-decane in the RCM experiments. We examined one possible explanation; it is likely that n-decane reacts to some extent during the last few milliseconds of the compression stroke, which would lead to experimental results for the ignition delay time that are too short. We carried out calculations for reaction during the compression stroke and found that some, but not all, of the differences between the Kumar et al. and the other results for ignition delay could be attributed to their neglect of reaction during the compression stroke. Past studies of RCM ignition of n-heptane [90] showed considerable amounts of fuel consumption during the compression stroke in the Leeds University RCM, which has a relatively rapid compression stroke. Slower compression strokes would make this effect larger. There is also some experimental variation in the measurements in both the RCM and the shock tube that might produce some disagreement. The novel construction of the Case RCM, to reduce the effects of wall boundary layers on the ignition, may also not yet be fully understood and may be contributing to the uncertainties. The low vapor pressure of n-decane also makes it challenging to prepare a precise amount of fuel and air for the RCM. Further comparisons between the Case RCM and results from other RCM facilities with fuels for which reliable kinetic mechanisms exist, are recommended to resolve some of these effects.

High temperature shock tube experiments - 2

Zhukov et al. [82,83] reported results of ignition delay experiments for stoichiometric and lean mixtures of n-decane in air behind reflected shock waves. Stoichiometric mixtures at 13 and 80 atmospheres pressure and lean ($\phi = 0.5$) mixtures at

78 atm. were included. Zhukov et al. compared their experimental ignition delay times with those of Pfahl et al. [85] with generally good agreement, at both 13 and 80 atm pressures. The measured ignition delay times were compared with computed values, using four different reaction mechanisms using EXGAS [27-31], Bikas and Peters [13], Lindstedt and Maurice [53,54] and Zhao et al. [48,49]. The mechanism of Zhao et al. was unsuccessful in reproducing the experimental results, due to the lack of low temperature reaction pathways which are important at the conditions of the experiments, and the other mechanisms provided results that were judged inaccurate by Zhukov et al., largely due to computed ignition delay times that were too long.

We used the present n-alkane mechanism for n-decane to simulate the shock tube experiments of Zhukov et al. The results at 13 atm pressure, for stoichiometric mixtures of n-decane and air, are summarized in Fig. 13. Similar to the model results, using the mechanism of Bikas and Peters, reported by Zhukov et al., our computed ignition delay values were longer than the measured results by factors about 1.5, with a larger difference for the lowest temperature point. Similar results were obtained for the higher pressure (~ 80 atm) experiments for $\phi = 0.5$ and 1.0, shown in Figures 14 and 15. In all three cases, it appears that the computed results are longer than the measured values by a modest margin. Both experiments and model calculations show a distinct NTC behavior for the stoichiometric mixtures in Fig. 15 but little or no NTC behavior at f = 0.5. For the stoichiometric mixtures, the model and experimental results are in good agreement at both high and low temperatures, but the experiments display more NTC behavior than do the model results.

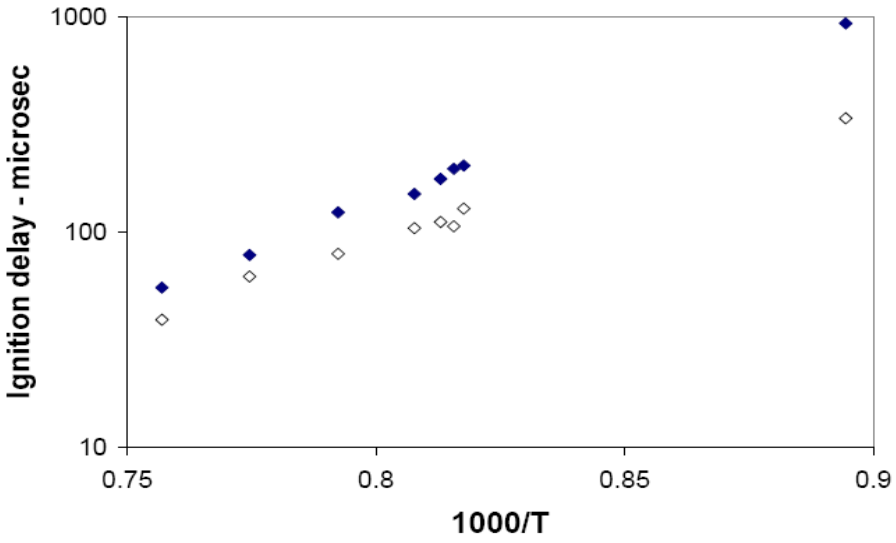

Fig. 13. Computed and experimental ignition delay times for $\phi = 1$, n-decane/air at 13 atm pressure. Experiments (◊) from Zhukov et al. [82,83], present model (♦).

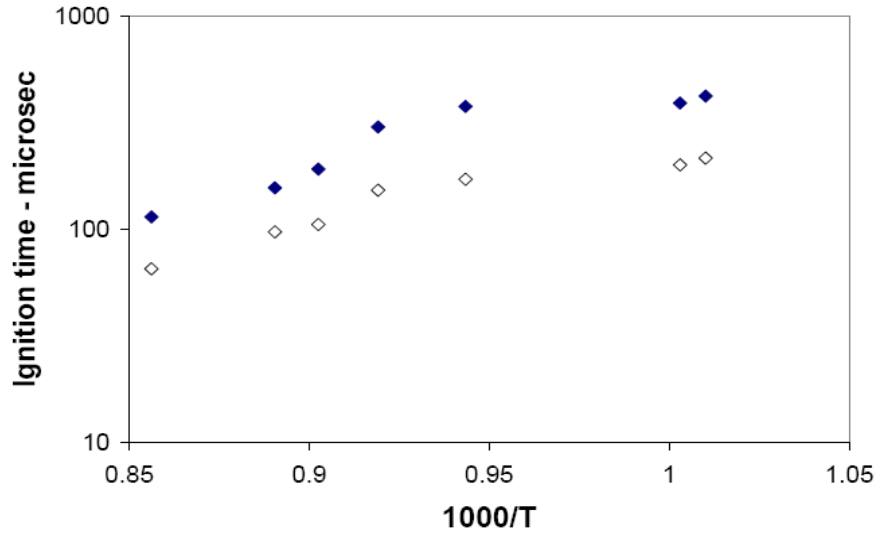

Fig. 14. Computed and experimental ignition delay times for $\phi = 0.5$, n-decane/air at 80 atm pressure. Experiments (◊) from Zhukov et al. [82,83], present model (♦).

In order to put the shock tube results of Zhukov et al. into context with the other high pressure shock tube and RCM ignition experiments and modeling results, we included the Zhukov et al. data into the same plot as in the analysis above for the other

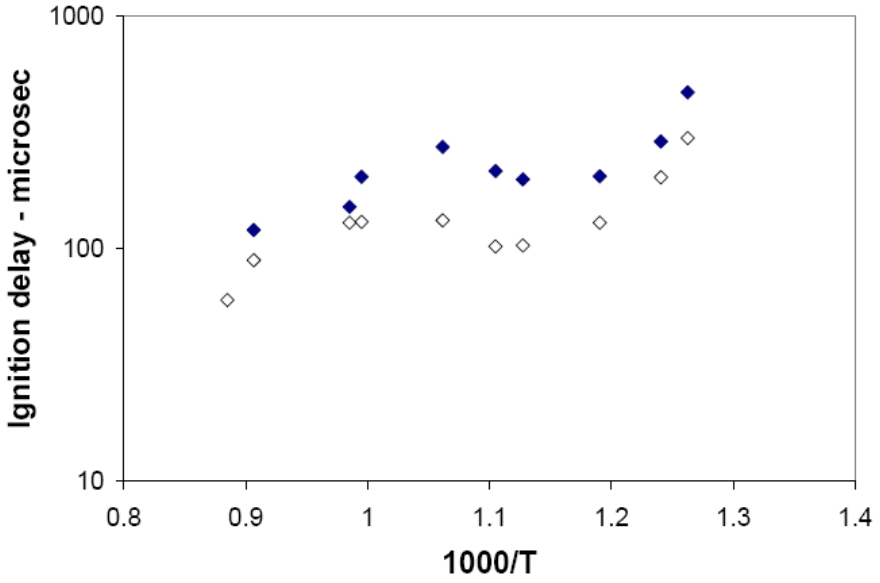

Fig. 15. Computed and experimental ignition delay times for $\phi = 1.0$, n-decane/air at 80 atm pressure. Experiments (◊) from Zhukov et al. [82,83], present model (♦).

experiments, as shown in Fig. 16 with all the data measured at approximately 13-14 bar and, in the cases of Kumar et al. [86] and calculations of Bikas and Peters [13], extrapolated slightly from $\phi = 0.8$. The experiments of Zhukov et al. and the computed ignition delay times, using the present n-alkane mechanism, are shown at the highest extent of the temperature range covered in Fig. 16. At this degree of analysis, it appears that the experimental results of Zhukov et al. and the present modeling results are well within the expected ranges established by all of the other experiments and model calculations. The differences between modeling calculations and the individual Zhukov et al. measurements in the other figures above are evidently not significant. Although not shown in Fig. 16, the computed results reported by Zhukov et al.,

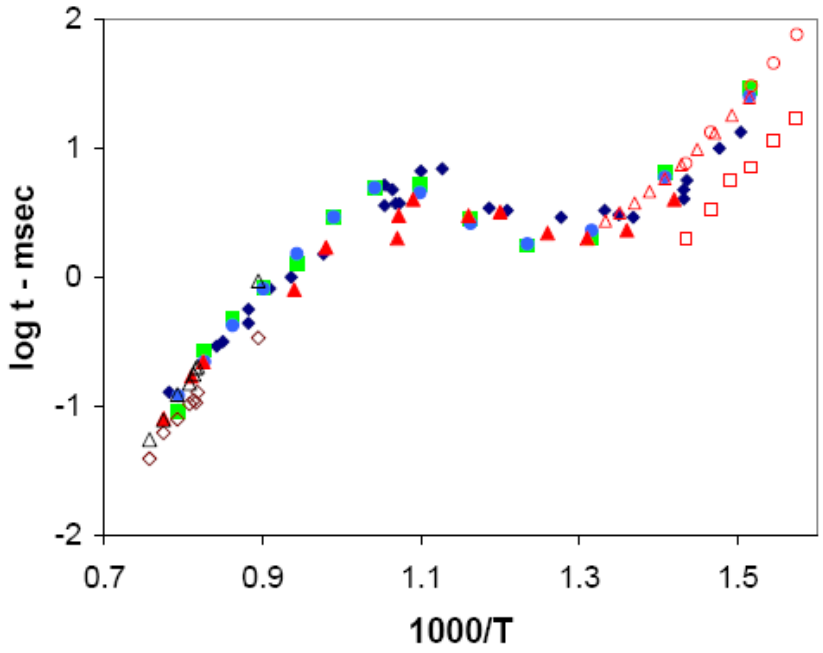

Fig. 16. Ignition delay times for stoichiometric n-decane in shock tubes and rapid compression machines at approximately 14 bar pressure. Experimental high temperature shock tube results from Zhukov et al. [82,83] shown by (◊), present model by (Δ). All other symbols are the same as in Fig. 12.

using reaction mechanisms from Bikas and Peters [13] and Lindstedt and Maurice [53,54] at 13-14 bar pressure, are also within the scatter of data at the highest temperatures plotted in Fig. 16.

The conclusions are somewhat different for the higher pressure ignition experiments of Zhukov et al. The experimental results at $\phi = 1$ and 80 bar pressure are summarized in Fig. 17, together with the computed results from the present n-alkane mechanisms. Also shown are the experimental results from Pfahl et al. [85] at 50 bar pressure and $\phi = 1$ and the corresponding computed results, again using the present n-alkane mechanism. The two sets of experimental and modeling results show some similarities. Both model and experiments show that ignition becomes faster as the pressure increases, and the amount of change in the experiments as pressure changes

from 50 to 80 bar is reproduced well by the mechanism. In addition, the amount of NTC behavior seems to decrease as pressure increases, although the temperature range over which NTC behavior is observed seems to be nearly the same at 50 bar as at 80 bar.

However, at both pressures, the computed results are longer than the experimental values by about a factor of 2-3. The differences between experimental and modeling results seem about the same at 80 bar as at 50 bar, so the model accurately reproduces the pressure dependence of ignition delay over this range of pressures, but these high pressure ignition curves do not converge to a single overall picture such as that for 13 bar pressureshown in Fig. 16. As a result, we must conclude that the kinetic mechanism

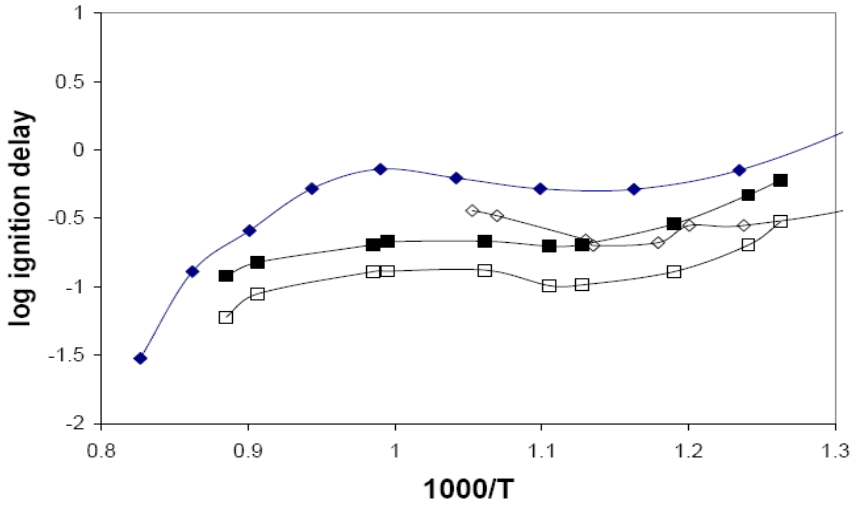

Fig. 17. Comparisons of shock tube experimental and computed ignition delay times of Zhukov et al. [82,83] at 80 bar (□)and Pfahl et al. [85] at 50 bar (◊), for n-decane at ϕ=1. Filled symbols show corresponding computed results.

does not correctly reproduce the observed results of these ignition events at very high pressures, and further study of both the kinetic reaction pathways and the experimental results is required. Further experimental results at elevated pressures would be very helpful in resolving these important differences.

Flow reactor experiments

Zhao et al. [48,49] carried out pyrolysis and oxidation experiments for n-decane in the Princeton flow reactor at atmospheric pressure, measuring a wide range of intermediate and product concentrations as functions of time. They also produced reduced and skeletal kinetic mechanisms that did a very respectable job of reproducing many of the species levels.

The pyrolysis experiment used 1456 ppm n-decane in nitrogen at an initial temperature of 1060K and found ethene, propene and larger 1-olefins as major products, in addition to methane, ethane and acetylene. The computed species concentrations for n-decane and the major products are shown in Figure 18. Comparisons between experiments and measurements are also excellent for methane and 1,3-butadiene, while computed results are lower than the experiments by a factor of 2 for 1-butene and higher than the experiments by a factor of 2 for 1-pentene.

Comparisons between computed and experimental results for an oxidation case are shown in Figures 19 and 20. The mixture is stoichiometric and dilute, with 1452 ppm n-decane, at an initial temperature of 1019K and 1 bar pressure. The major products are ethene, carbon monoxide, 1-butene, propene, methane, 1-hexene, ethane and 1,3-butadiene, and the model shows good agreement with experimental results, except for CO, with the computations showing an earlier rise in CO concentration than in the experiments. We note that the skeletal mechanism of Zhao et al. [48,49] showed the same rise in CO concentrations earlier than the experimental results as shown in Fig. 19.

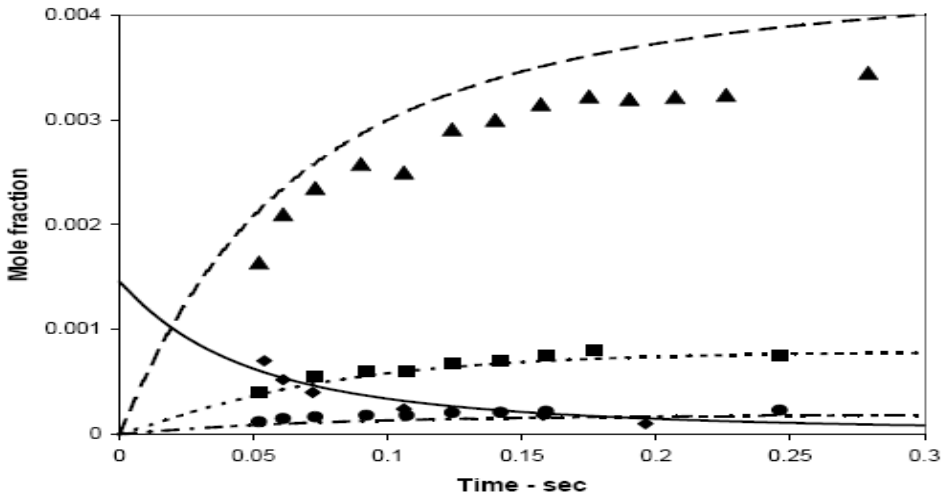

Fig. 18. Fuel and major pyrolysis products of n-decane in the Princeton flow reactor [48,49], 1456 ppm n-decane, 1060K, 1 atm. Lines show computed results, symbols show experimental results. Ethene (▲, dashed line), propene (■, dotted line), n-decane (♦, solid line), ethane (●, dot-dash line)

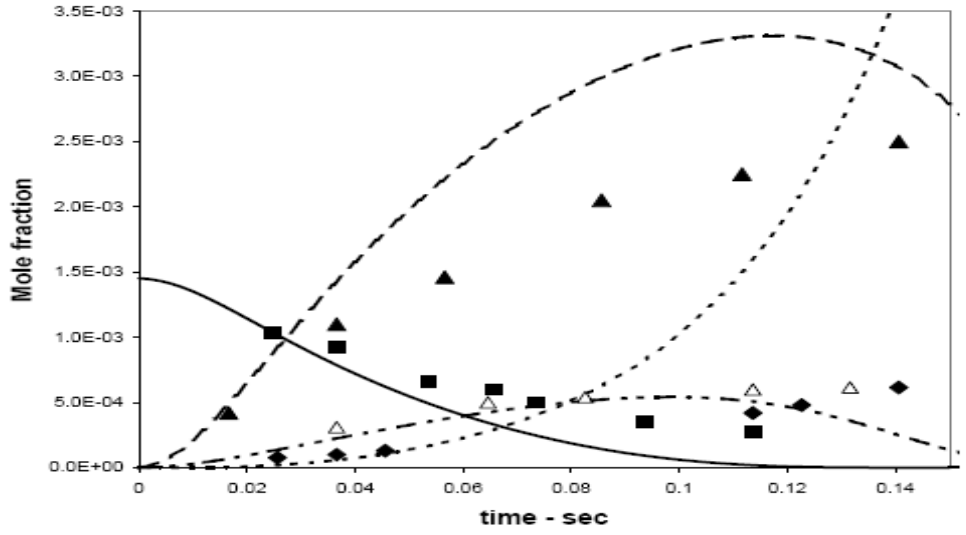

Figure 19. Major species concentrations for n-decane oxidation, To = 1019K, 1452 ppm n-decane, $\phi = 1.0$, 1 atm. Lines show computed results, symbols show experimental results [48,49]. n-cetane (■, solid line), ethene (▲, dashed line), CO (♦, dotted line), propene (Δ, dash-dot line)

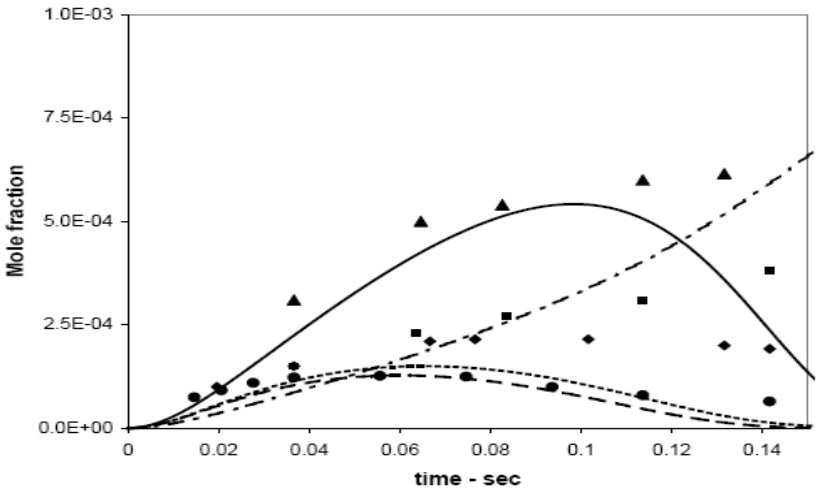

Figure 20. Intermediate species concentrations in n-decane oxidation, same conditions as Fig. 19. Lines show computed results, symbols show experimental data [48,49]. Propene (▲, solid line), methane (■, dot-dash line), 1-butene (♦, dotted line), 1-hexene (●, dashed line)

The Princeton flow reactor has a long and successful history of kinetic studies of the intermediate temperature range. In distinction with the low temperature range for hydrocarbon oxidation where the alkylperoxy radical isomerization reaction pathways are most important, and the high temperature range where H atom reactions with O_2 are most important, in the range of 900 - 1100K where most flow reactor studies have been done, the dominant radical is frequently HO_2. This was seen to be the case in these n-decane simulations, and comparisons between computed and experimental results provide a unique opportunity to test the rates of H atom abstractions from the fuel by HO_2.

Jet stirred reactor experiments

Dagaut and collaborators have carried out an extensive series of experimental and kinetic modeling studies of oxidation of large hydrocarbons in a jet-stirred reactor, measuring many intermediate species concentrations over broad ranges of operating conditions that are very useful for kinetic mechanism development and validation. In particular, studies of n-decane [40] and n-hexadecane [31,38,42] have been carried out to test high temperature reaction mechanisms for these fuels. Later, those kinetic mechanisms for n-decane and n-hexadecane were used to test the surrogate capabilities of those fuels to describe oxidation of kerosene and biodiesel fuels. Overall, the n-alkanes appeared to be very satisfactory as surrogates for these practical transportation fuels.

Dagaut and Cathonnet [55] have reviewed experiments and modeling for the combustion of kerosene, showing how n-decane was used for some time as a suitable surrogate for kerosene. They showed that the overall reactivity of kerosene is due to its large n-alkane fraction, so if the function of the surrogate is limited to simulation of the kerosene, then n-decane is a good substitute. However, n-decane was later replaced by a variety of multicomponent mixtures that include large alkyl benzenes and are able to reproduce the production of benzene and other small aromatic intermediates and the formation of soot under some conditions. The role of large aliphatic compounds in kerosene, other jet fuels, and diesel fuel is still very important for ignition and energy release simulations, and the jet-stirred reactor experiments of Dagaut et al. are important for mechanism validation of several different large n-alkanes.

In the present work, experiments with n-decane and n-hexadecane oxidation are used to test the capabilities of the present n-alkane reaction mechanisms. For n-decane,

experimental results are available for pressures at 1, 10, 20 and 40 atm, equivalence ratios from 0.2 to 1.5, residence times from 0.1 to 1.0 seconds, and a number of inlet concentrations of n-decane. In order to keep the reaction from proceeding too rapidly and forming flames or exploding, the total mixture is kept very dilute. For illustration and to demonstrate the level of mechanism validation that is possible with these experiments, below we shall show comparisons between experimental and computed results for one stoichiometric mixture at 10 atm pressure and three additional cases for lean, stoichiometric and rich mixtures at atmospheric pressure.

The first test was reported by Dagaut et al. [39] in a study of kerosene combustion at pressures from 10 to 40 atm pressures, in which n-decane was used as a surrogate for the kerosene for kinetic modeling purposes. The kinetic model was intended for high temperature systems and reproduced the observations quite well for most species n-decane. The first specific example used here is intended to show the mechanism capabilities at elevated pressures and describes a dilute (1000 ppm fuel) stoichiometric mixture of n-decane and oxygen, at 10 atm pressure and a residence time in the stirred reactor of 0.5 seconds. Figure 21 shows the computed and experimental values for 5 species for which measured values were reported, with good agreement between model and experiment.

Other interesting kinetic information from this simulation includes the relative levels of the c10 olefins and the 1-olefins for species with fewer than 10 carbon atoms. The decenes are shown in Figure 22, together with the concentration of the n-decane fuel.

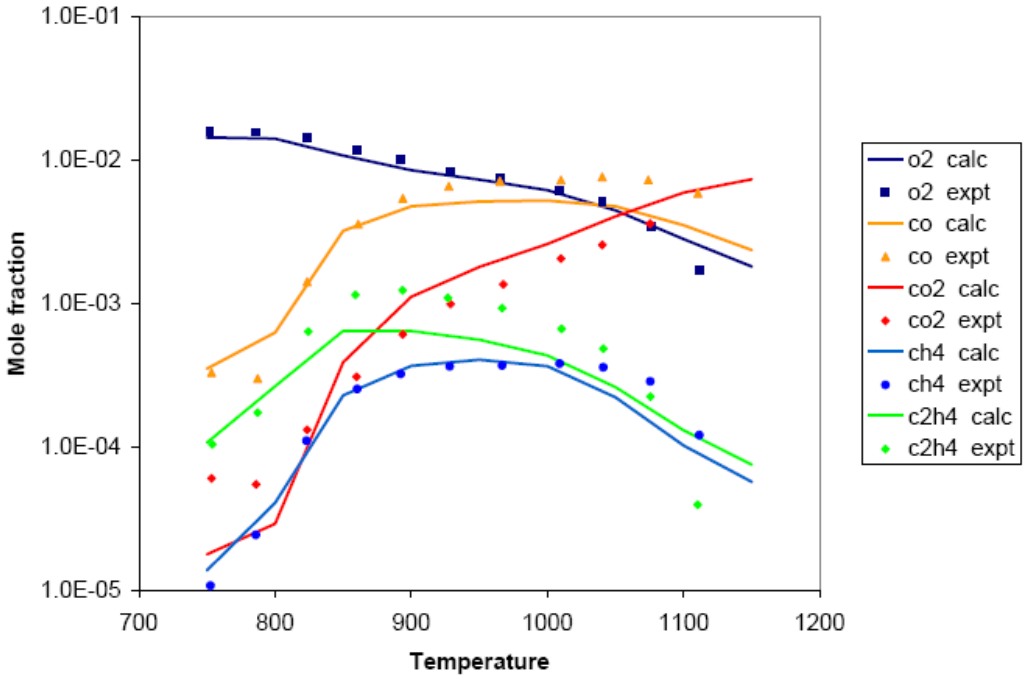

Fig. 21. Chemical species concentrations in a jet stirred reactor oxidation of n-decane, 10 atm pressure, 1000 ppm n-decane, $\phi = 1.0$, residence time of 0.5 s. Lines represent computed values, symbols are experimental results [39].

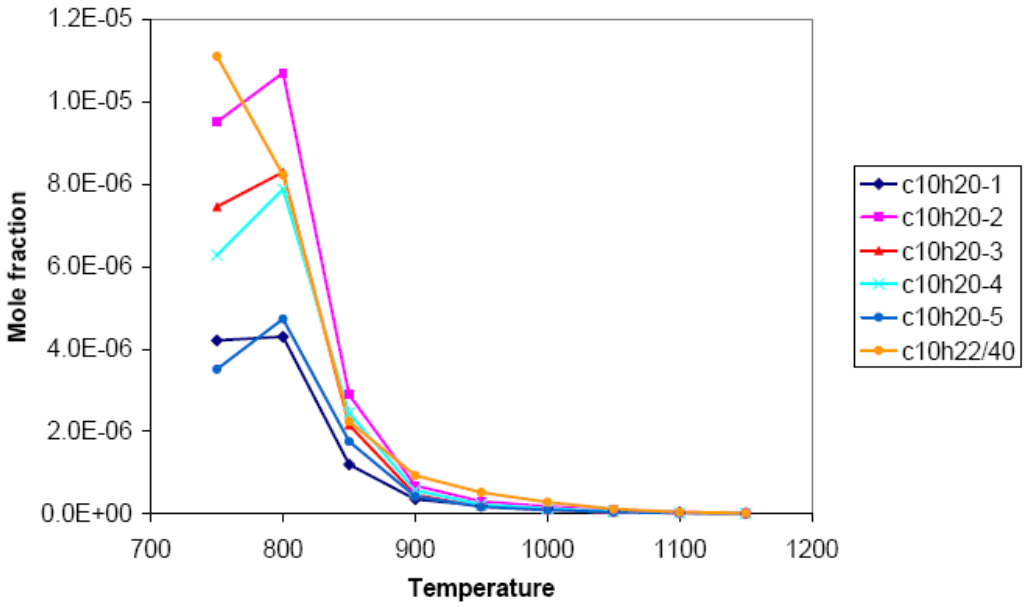

Figure 22. Computed levels of decenes produced in oxidation of n-decane in jet-stirred reactor, same conditions as in Fig. 21. Concentration of n-decane is shown for comparison.

The decenes have their highest concentrations at relatively low temperatures, where the fuel consumption rate is greatest. Production of conjugate olefins during n-alkane oxidation is relatively difficult because it requires breaking a C-H bond following H atom abstraction from the fuel, rather than breaking a C-C bond via β-scission or addition of molecular oxygen, both of which are faster at temperatures around 800K. The 1-decene is produced at low rates because it requires breaking a primary C-H bond with its higher bond energy than secondary C-H bonds. The 5-olefin also is produced at low levels because it has only one reaction sequence for production, in contrast to the multiple formation pathways for the 2-, 3-, and 4-decenes.

In contrast, for all of the olefins with fewer than 10 carbon atoms, the present mechanism predicts that the 1-olefins have much higher concentrations than the other olefins with the same number of carbon atoms. Thus, for example, 1-octene is much more abundant than 2-octene, 3-octene or 4-octene in the n-decane simulations. This trend is easy to explain as a result of β -scission of alkyl radicals produced from H atom abstraction from n-decane, and the pattern is observed for combustion of all of the n-alkanes in both kinetic modeling and experiments.

The relative concentrations of 1-olefins produced from n-decane are shown in Figure 23, showing that those olefins with multiple production reaction pathways have much higher concentrations than those with more limited production pathways with higher energy barriers. Note that the c9 1-olefin, like the 1-decene discussed above, has a very low concentration, due to its unique production path which requires abstraction

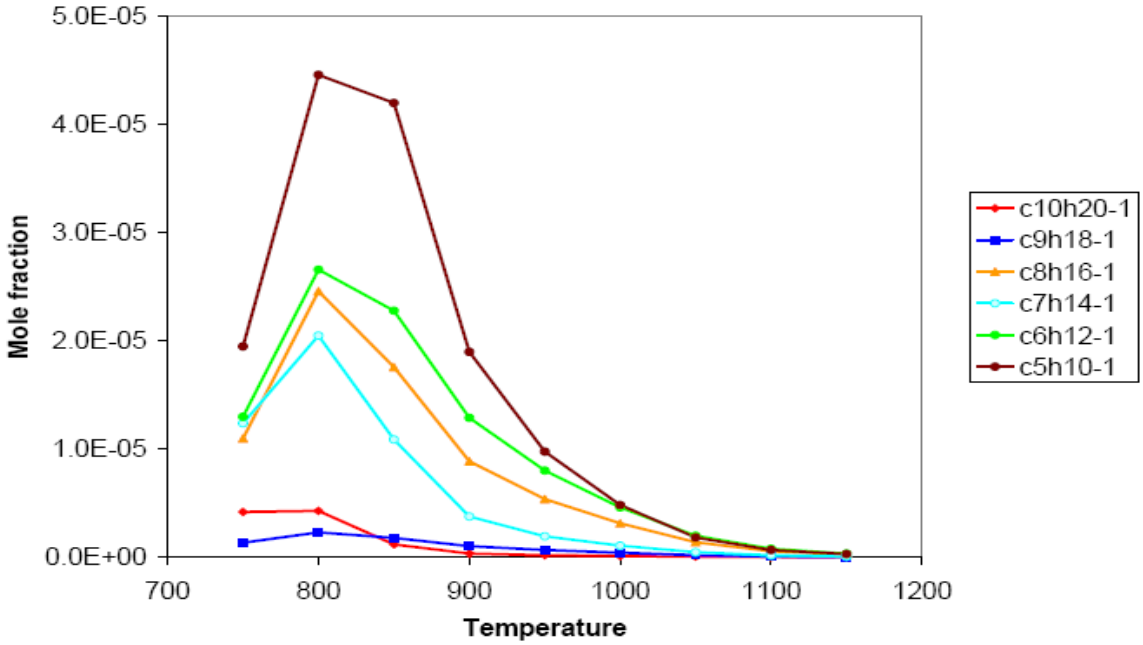

Figure 23. Concentrations of 1-olefins produced during oxidation of n-decane in a jet-stirred reactor. Same conditions as Fig. 21.

of an H atom from the 3-site in n-decane followed by breaking the C-C bond between the first and second carbon atoms in the linear chain.

Experimental and computed results were reported for stirred reactor oxidation of n-hexadecane by Ristori et al. [38,42], and additional kinetic analysis and modeling of the same experiments were reported by Fournet et al. [31]. The present kinetic mechanism for n-hexadecane was used to calculate the species profiles for each of the n-hexadecane experiments, which included mixtures at ϕ = 0.5, 1.0 and 1.5, all with initial mole fraction of n-hexadecane of 0.03%, diluted in N_2, at atmospheric pressure, over a temperature range from 1000K to 1250K, with a residence time of 0.07 s. The same experiments were used to validate the previous modeling studies of Dagaut et al. [38,42] and Fournet

et al. [31], and the agreement between the experimental data and the present computed results was good, and very comparable to those previous studies. Examples of these comparisons are shown in Fig. 24 for several of the measured chemical species, for the case at $\phi = 1.5$.

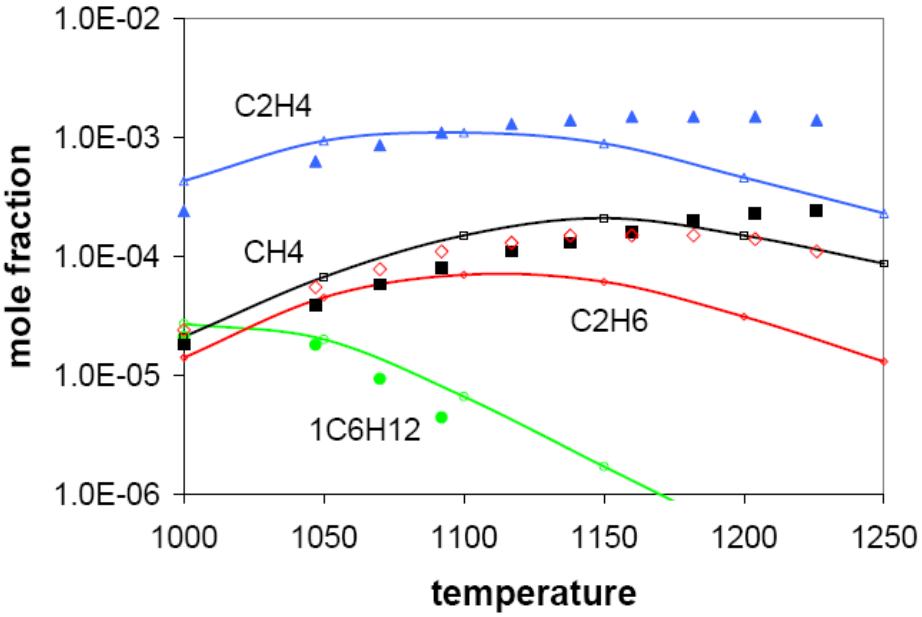

Fig. 24. Comparison between computed and experimental [38] results for selected species in n-$C_{16}H_{34}$ oxidation in a JSR. Conditions are $\phi = 1.5$, 1 atm pressure, and 0.07 s residence time.

These are complex mechanisms for such large fuel molecules, and judging only from the JSR simulations, it appears that the mechanism produces the observed intermediates with reasonable accuracy, but there are many areas in which greater precision is desirable, and a considerable amount of further study is needed.

Recently, Dagaut et al. [45] used a kinetic mechanism for n-hexadecane to simulate combustion of rapeseed methyl ester (RME) biodiesel fuel in a JSR. The overall agreement between experimental RME species measurements and computed species

levels for n-hexadecane fuel was very good. The largest disagreement was for CO_2 at temperatures below 1100K, where the experiments indicated concentrations of CO_2 much higher than the computed values. These simulations were repeated with the present n-hexadecane kinetic mechanism, with initial mole fractions of 0.0005625 n-$C_{16}H_{34}$, 0.011 O_2 and N_2 diluent. and the results for the major species are shown in Fig. 25.

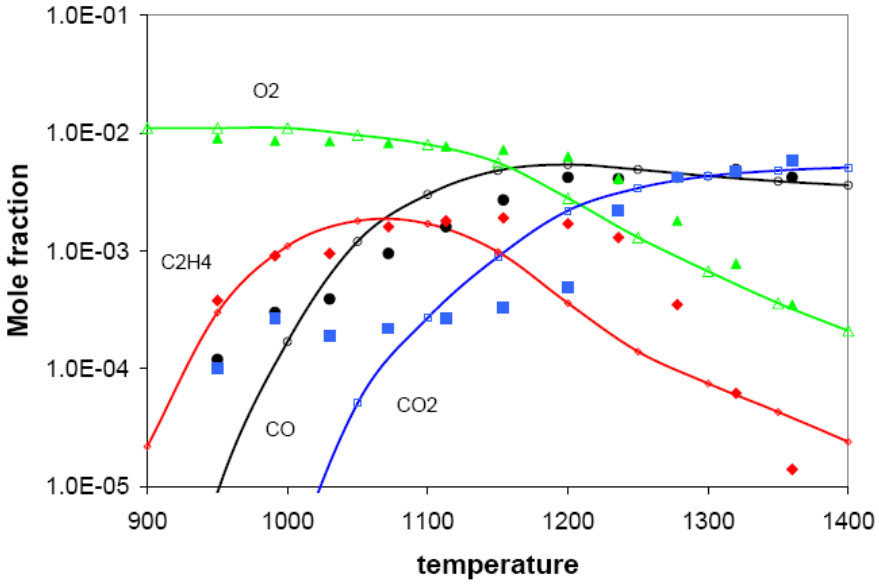

Fig. 25. Major species profiles in JSR oxidation, comparing RME experiments [38] and present n-hexadecane model. Conditions are 1 atm, 0.07 s residence time.

As in Dagaut et al. [45], the overall agreement is very good. Similar agreement was observed for most other species; for example, the computed level of 1-C_6H_{12} reached a peak mole fraction of 6 x 10^{-5} at 1000K, and the peak mole fraction of the same species was measured to be 4 x 10^{-5} at the same temperature. Also in agreement with Dagaut et al., the most significant difference between calculations and experiments was found to be the CO_2 levels at lower temperatures as seen in Fig. 25. This difference is due to the methyl ester group in RME, which produces CO_2 at temperatures below 1100K directly during fuel decomposition, rather than via oxidation of CO, which is delayed until higher

temperatures during oxidation of n-hexadecane. Low temperature production of CO_2 from a methyl ester group has been observed in other large methyl ester fuels [91], and the peak in CO2 mole fraction at 950K - 1000K in Fig. 25 is a "signature" of methyl ester oxidation that is not reproduced during oxidation of n-alkanes. Otherwise, it appears that n-alkanes can reproduce many of the combustion characteristics of large methyl esters, as first shown by Dagaut et al. [45].

In a series of jet-stirred reactor experiments, with accompanying high temperature kinetic modeling, Dagaut et al. [40,42] reported results from a family of n-decane/O_2/N_2 mixtures, with very dilute inlet fuel concentrations (700 ppm n-decane) over a wide range of oxygen concentrations from lean to very rich.

We then used the kinetic mechanisms for all of the n-alkanes to carry out a series of numerical experiments under the same jet-stirred reactor conditions as those reported above for 700 ppm n-decane by Dagaut et al. [40,42], at atmospheric pressure, residence time of 0.07s, $\phi = 1.0$. We calculated stoichiometric cases for n-octane, n-decane, n-dodecane, n-tetradecane and n-hexadecane. We scaled the inlet concentrations for each n-alkane to match the carbon atom flux with that for n-decane; therefore the inlet levels were (n-octane/O_2) = (875 ppm/10938 ppm), for n-decane (700 ppm/10850 ppm), for n-dodecane (583 ppm/10750 ppm), for n-tetradecane (500 ppm/10750 ppm), and for n-hexadecane (438 ppm/10718 ppm). This approximately also scales the total H atom flux, although the H atom amounts change slightly while the carbon content remains constant.

The results of the jet-stirred reactor calculations are shown in Figure 26, showing the fuel concentrations for n-octane, n-decane and n-dodecane, under conditions of constant C atom input flux.

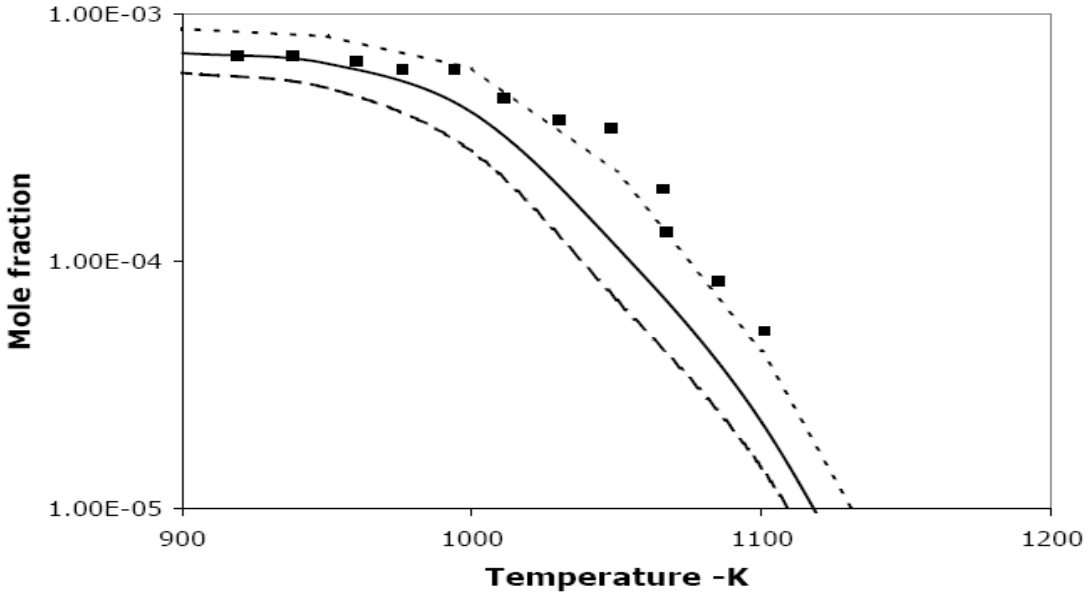

Fig. 26. Fuel concentrations in jet-stirred reactor simulations. Initial values are scaled to 700 ppm in n-decane for comparison. Mixtures are stoichiometric, 10 atm pressure, residence time of 0.07 s. Experimental values are shown for n-decane (symbols) [40,42].

The fuel mole fraction curves are different in order to keep the carbon flux constant for all of the mixtures, but a much different result is observed for nearly all of the other species in the group of calculations, as shown in Figure 27 in which the levels of ethene, methane and 1-butene are plotted. The computed concentrations of these species, and most others not shown, are very nearly equal to each other, regardless of the n-alkane fuel being used. Experimentally measured values for the n-decane case are shown in Fig. 27. From these results, it appears that any large n-alkane fuel could serve as a reliable surrogate for any of the others, as long as the fuel level is properly scaled. In this case, n-octane, n-dodecane, n-tetradecane and n-hexadecane all predict the same values for the major intermediates shown in Fig. 27 and for most other species as well. Accordingly, n-

octane or n-decane would be very acceptable surrogates for a larger fuel such as n-hexadecane, thereby reducing significantly the computational costs of kinetic simulations. The only species not reliably simulated with this approach are the larger stable species associated with the larger fuel that are not included in the mechanism for the smaller surrogate fuel.

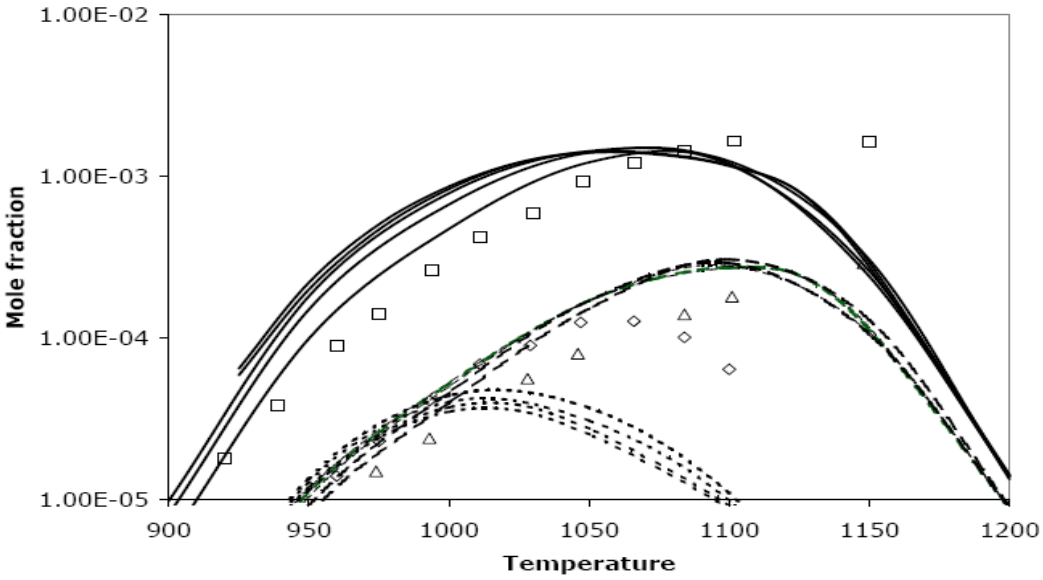

Fig. 27. Computed concentrations of ethene (solid lines), methane (dashed lines) and 1-butene (dotted lines) for n-alkane fuels under jet-stirred reactor conditions. Symbols represent experimental values from Dagaut et al. [42] for n-decane oxidation, ethene (□), methane (◊), and 1-butene (Δ).

In computed results when the fuel is n-decane, concentrations of the n-decane fuel products 1-decene and 1-nonene are very small due to their small production rates via limited reaction pathways, as seen in Fig. 23. Concentrations of those 1-olefins would not be small if the fuel were n-dodecane or n-hexadecane. Therefore n-decane would be expected to predict reliable levels of 1-octene and smaller 1-olefins but not for 1-decene

or 1-nonene if n-decane were used to simulate results for n-hexadecane or another larger n-alkane.

As noted by Dagaut and Cathonnet [55], n-decane can reproduce the overall reactivity, heat release and many intermediate species levels in combustion of kerosene jet fuel, but this approach is still unable to address other questions such as sooting and the influences of aromatic species in the kerosene fuel. When the fuel itself includes significant amounts of aromatic species, then use of a multicomponent surrogate mixture which includes a relevant aromatic compound is required. For this reason, Dagaut and Cathonnet included n-propyl benzene and n-propyl cyclohexane with n-decane to provide a more realistic kerosene surrogate.

High pressure flow reactor experiments

Agosta et al. [92] used a pressurized flow reactor to study autoignition and combustion of several components of a proposed surrogate jet fuel. One of the components was n-dodecane, and they used a semi-detailed kinetic model to analyze their measured results, showing reasonably good agreement. Related analysis of the same measurements was carried out in a larger study of semi-detailed kinetic mechanisms by Ranzi et al. [57]. We have used the same experimental data to test the present mechanism for n-dodecane.

The experiments on n-dodecane were carried out at 8 atm pressure for dilute lean mixtures. The inlet temperature of the reactants and nitrogen diluent was varied slowly from about 900K down to about 600K, and the overall reactivity was determined by measuring the CO concentrations in the reacting gases after an experimental residence

time of 120 ms. The time constant for the inlet temperature variation is much longer than the reactant residence time in the flow reactor, so the reacting conditions are assumed locally time independent. Detailed simulations of these pressurized flow reactor experiments focused on one case at an equivalence ratio of 0.2 and another case at ϕ = 0.3, and the resulting CO results are compared with the experimental data in Figure 28.

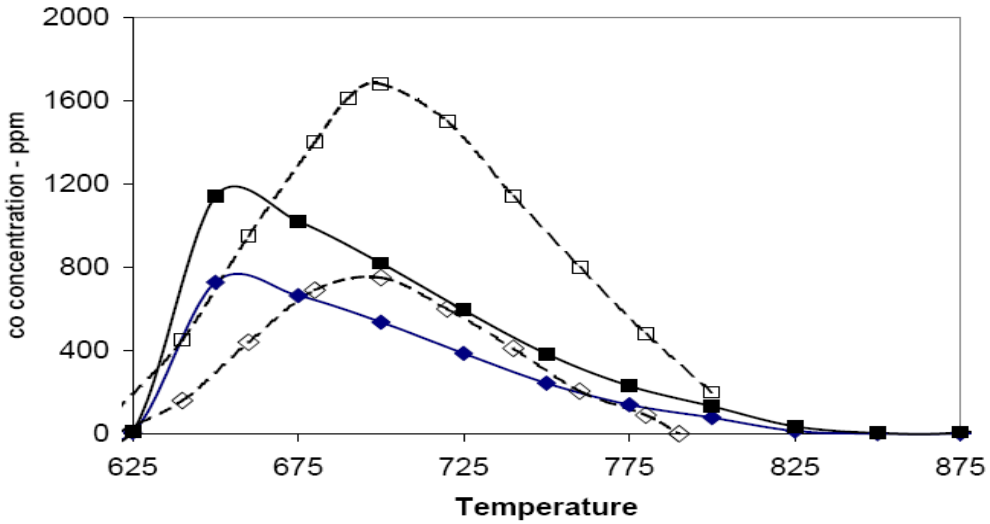

Fig. 28. Computed and experimental CO concentrations in pressurized flow reactor [92], at 8 atm, residence time of 120 ms. Computed values are shown for curves with filled symbols, experiments with open symbols, ϕ = 0.2 (◊ and ♦), and ϕ = 0.3 (□ and ■).

All n-alkane oxidation in the temperature range of these pressurized flow reactor experiments is strongly influenced by low temperature, alkylperoxy radical isomerization kinetics, and production of CO is close to the end of that reaction sequence. The degree of agreement between measured and computed values in Fig. 28 is a very demanding test of the validity of the kinetic mechanism. At both values of equivalence ratio, the kinetic model shows that the peak reaction zone is shifted slightly towards lower temperatures, compared to the measurements. The same type of shift toward lower temperatures was

observed by Ranzi et al. using their semi-detailed or lumped kinetic model, although the shift was less in their simulations than that shown in Fig. 28. The good agreement in the absolute peak levels of CO also provides support for the reaction mechanism.

N-alkane thermolysis

Large n-alkanes are of considerable interest in various process engineering applications. As a result, there are many studies of conversion of n-alkanes to other chemical species as potential products, and one such study was selected for mechanism validation. In this study by Zhou et al. [93], n-alkane thermal pyrolysis, or thermolysis, of n-nonane, n-dodecane, n-tridecane, and n-hexadecane was studied at temperatures from 623K to 893K at atmospheric pressure.

Under these conditions, 10% - 40% of the n-alkane fuel was consumed, leading primarily to 1-olefins from ethene up to the 1-olefin with the same number of carbon atoms as the n-alkane fuel. Overall, yields of 1-olefins decreased with increasing molecular weight; very little of the 1-olefin with the same number of carbon atoms as the fuel was produced, and the next-smaller 1-olefin production was also quite small. These trends are very similar to those for 1-olefin production noted above in the jet-stirred reactor discussion in Figs. 22 and 23.

Computed results for product distributions are compared with the experimental results in Figure 29 for n-dodecane at atmospheric pressure and 893K. The overall agreement is quite good, and the kinetic model correctly identifies ethene as the major product, although the model overpredicts its absolute level. The highest concentration large 1-olefin is 1-c6h12 in both the model and the experiments, and although not shown

in the figure, the levels of 1-undecene and 1-dodecene are very small in both the experiments and the calculations. The main difference between the experimental and computed results is that the experimental results were obtained after a residence time of 3.3 seconds, while the model predicted the same conversion of n-dodecane after only 1 second.

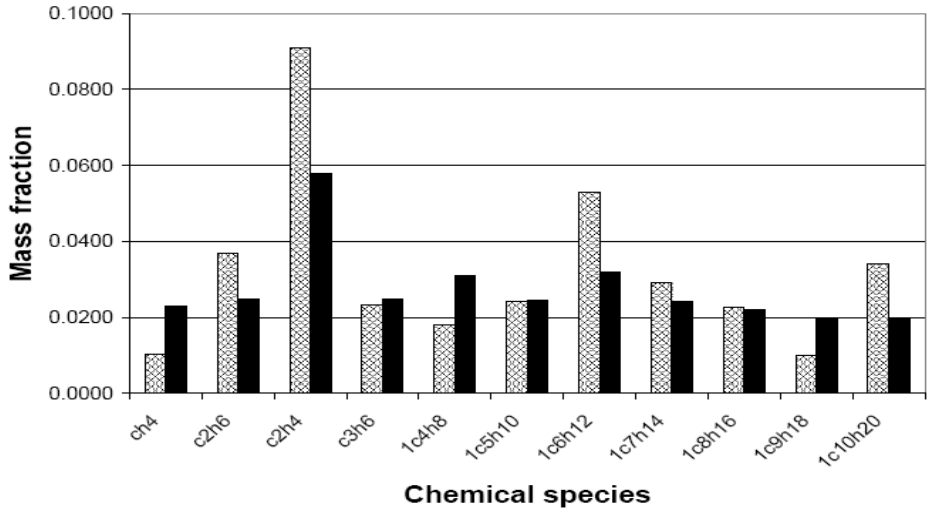

Figure 29. Products of n-dodecane thermolysis at 893K, experiments from Zhou et al. [93] at 1 atm, with 35.6% conversion of the fuel. Residence time for experiments is 3.3 s, for computed results 1.0 s. Experimental results are solid bars, computed results shaded.

Similar agreement was observed for thermolysis of n-nonane, shown in Fig. 30. Again, most of the predicted product levels are quite close to the experimental results, while the ethene level is again overpredicted by the model. In the case of n-nonane, the experimental time required for 9.3% conversion is 1.5 seconds when the product concentrations were measured as shown in Fig. 29, while the model produced the same n-nonane conversion in about 0.5 seconds. so the rates of conversion in the model appear to

be approximately three times greater than in the experiments, although the product distributions are very similar between the model and the experiments.

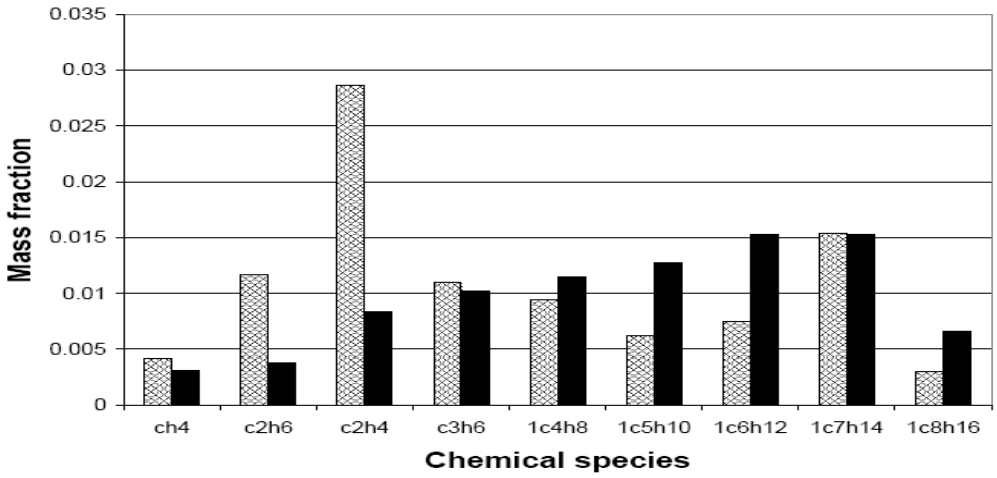

Figure 30. Products of n-nonane thermolysis at 893K, experiments from Zhou et al. [93] at 1 atm, with 9.3% fuel conversion. Residence time for experiments is 1.5 s, for computed results 0.5 s. Experimental results are solid bars, computed results are shaded.

Pyrolysis of n-dodecane

Herbinet et al. [51] carried out a series of gas-phase pyrolysis experiments, using 2% n-dodecane in 98% He diluent, in a jet-stirred reactor specially designed to study thermal decomposition of liquid hydrocarbons. Experiments were carried out at temperatures from 773K to 1073K, and concentrations of 32 chemical species produced during the pyrolysis were measured at residence times from 1 to 5 seconds. Species measured included hydrogen, small saturated and unsaturated hydrocarbons, a wide range of 1-alkenes, and a variety of small aromatic, polyaromatic and cycloparaffin species. Herbinet et al. also carried out modeling simulations of their experimental results, using a mechanism for combustion of n-dodecane produced from their EXGAS software [27-31], in which they included reaction pathways forming and consuming aromatic compounds.

Aromatics are a relatively minor product of the pyrolysis, and in our validation simulations, we did not include the aromatic or the cycloparaffin species formation reactions in order to focus on the n-alkane portion of the pyrolysis process.

At a residence time of 1 second, pyrolysis is slow for temperatures below 800K, proceeds more rapidly at higher temperatures, dominated by production of 1-alkenes in the temperature range from about 875K to 975K, and 1-alkenes are consumed rapidly at temperatures above 1000K. All of these features are reproduced very well by the present reaction mechanism. The major products of these experiments were hydrogen, methane, ethene, and propene, followed by a series of 1-alkenes from ethene to 1-undecene, with smaller levels of aromatic and cyclic paraffins, and a sample of these results are shown in Figure 31. Percent conversion of n-dodecane and production of methane, ethene and propene all show excellent agreement between measured and computed values.

Most of the 1-alkenes larger than propene are somewhat overpredicted by the present mechanism, as seen from the 1-decene profile in Fig. 31, with very similar results for 1-hexene, 1-heptene, and 1-octene. However, the computed 1-undecene is slightly smaller than the experimental results, and the computed level of 1-nonene is also slightly smaller than the experimental values. It is possible that inclusion of formation reaction pathways for aromatics would reduce the 1-alkenes to levels closer to the experimental values, but we also investigated a reaction class not previously included in past mechanisms or the present models.

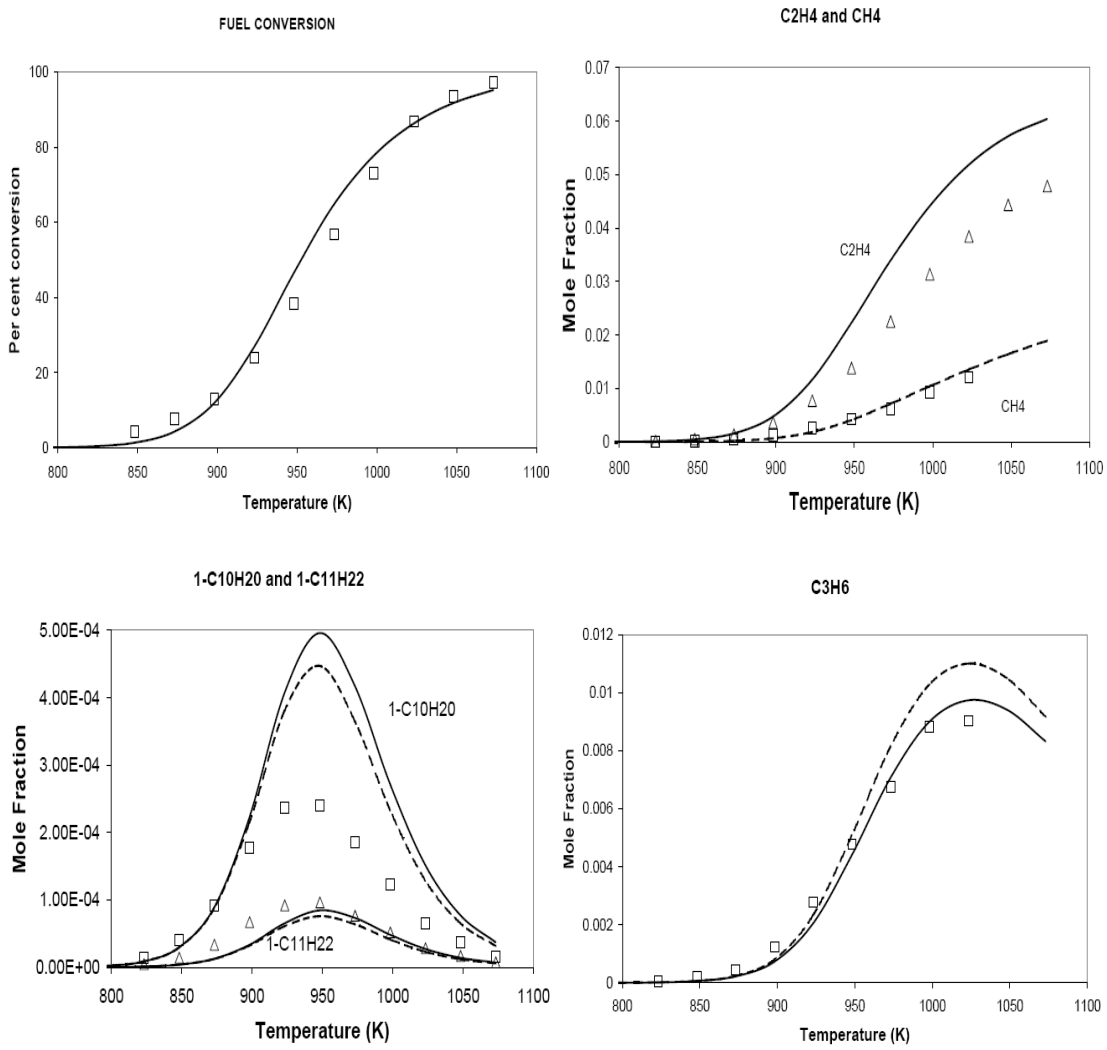

Fig. 31. Conversion of fuel and species produced in n-dodecane pyrolysis (2% n-dodecane, 98% He) at 1 second residence time for a range of temperatures. Experimental values [51] are shown as symbols, lines show computed results, dashed curves include retroene reactions of 1-alkenes.

Retroene reactions of the 1-alkenes were introduced into the mechanism of Herbinet et al. [51,52]. These reactions represent a unimolecular decomposition pathway, involving a 1,5 hydrogen shift followed by a dissociation into a smaller 1-alkene and propene. The A factors and activation energies are smaller than those for

unimolecular decomposition of 1-alkenes via C-C bond scission [76], and they contribute to 1-alkene consumption primarily over the range of temperatures in this study.

Inclusion of these retroene reactions in the present n-alkane mechanisms produced only a relatively small change in the computed levels of the large 1-alkenes illustrated in Fig. 31. Propene levels are increased when retroene reactions are included, since each reaction produces additional propene, and the computed concentrations of the larger 1-alkenes are reduced, since the retroene reactions provide additional consumption pathways for these species. For the 1-alkenes that are overpredicted by the original mechanism, these reactions improve the agreement between computed and experimental results, and for 1-undecene and 1-nonene the agreement deteriorates slightly. The influence of retroene reactions of the 1-alkenes has little effect on the computed levels of the major product species, except for propene where the agreement is poorer when these reactions are included. They also have little effect on the overall rate of n-dodecane conversion.

Herbinet et al. also included concentration measurements over a range of residence times during pyrolysis of some selected mixtures and temperatures, which provides a somewhat different validation task than the measurements described above at a fixed residence time. In one such experiment, a mixture with 2% n-dodecane and 98% helium, at a temperature of 973K and at atmospheric pressure was studied, with a large variety of species concentrations measured at residence times from one to five seconds. We simulated this experiment with the present reaction mechanism, and the results are summarized in Figure 32.

These results show the evolution of the pyrolysis experiment, with the initial fuel decomposition converting the fuel into large 1-alkenes from 1-undecane to 1-hexene as intermediate products. The 1-alkenes are subsequently consumed, producing smaller 1-alkenes, eventually producing ethene, propene, methane and hydrogen. The time-dependent 1-alkene concentrations all have the same overall shape, with an initial increase to an elevated level, followed by consumption and conversion to final products.

These experiments were simulated as described above with two versions of the mechanism. In the first simulations, the 1-alkene retroene reactions described above were not included, and then they were added for a second set of simulations. These results are shown in Fig. 32, showing the major products ethene and methane, and two of the 1-alkene intermediates, 1-decene and 1-hexene. The regular mechanism overpredicts the intermediate levels of most of the 1-alkene intermediate species concentrations, although computed profiles of the major products are quite accurate. When retroene 1-alkene species decomposition reactions were included, the peak 1-alkene concentrations were reduced and became much closer to the measured values, as shown in Fig. 32.

These retroene reactions compete with abstraction reactions and C-C bond-breaking reactions of the 1-alkenes, both of which produce radical species, while the retroene reactions produce only olefinic products that are much less reactive. As a result, the inclusion of these reactions reduces the radical levels and slows the overall rate of reaction. A result of this slower rate of reaction is the reduced production rates of ethene, methane and 1,3-butadiene shown in Fig. 32.

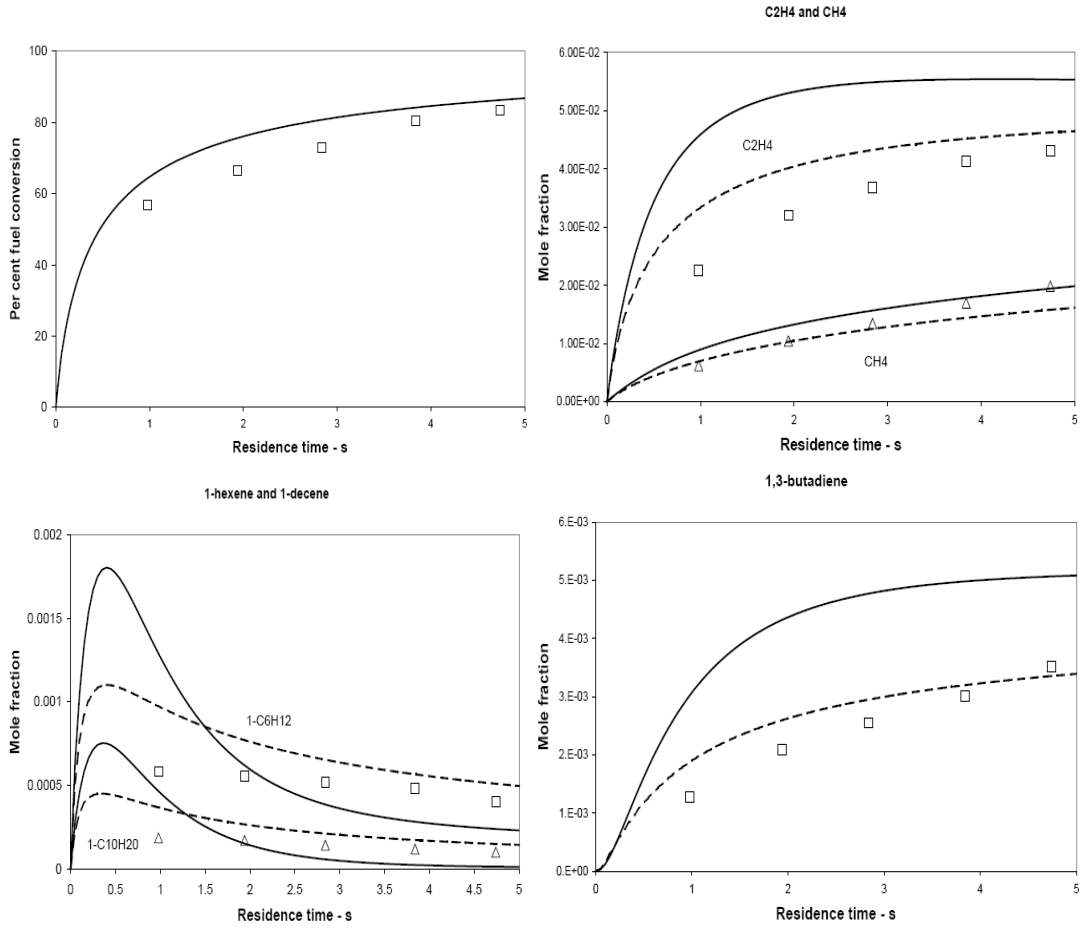

Fig. 32. Fuel conversion and species histories in n-dodecane pyrolysis [51] (2% n-dodecane, 98% He) . Temperature is 973K, symbols are experimental points, lines are computed results. Dashed curves include retroene 1-alkene decompositions, solid curves do not include them.

SUMMARY

Kinetic mechanisms for the large n-alkanes described and tested here extend to much larger n-alkanes modeling capabilities that have been available for n-heptane for some years. Attention has been given to providing the same level of kinetic detail that was contained in the previous n-heptane mechanism, so the experience that has been developed using the n-heptane mechanism is directly applicable to these larger fuels.

The greater size of the new mechanisms make mechanism reduction an even more serious challenge than before, so these mechanisms should provide a valuable set of mechanisms to test reduction systems. The lumping techniques of Dryer [48,49] and Ranzi [24,57] have already been applied to mechanisms similar to the present group.

These mechanisms also should be valuable in providing material for development of surrogate fuels [1-4] for practical systems as well as for unique systems such as biodiesel fuels. Large n-alkane species are prominent in transportation fuels, so the present mechanisms may be useful in making surrogate fuel mixtures more realistic than previously possible. A somewhat more subtle impact on surrogate fuel definitions has been provided by two of the n-alkane intercomparisons presented above that show that ignition and combustion of all of the n-alkanes from octane through hexadecane are remarkably similar. The ignition (see Fig. 6) and oxidation (see Fig. 27) of the n-alkanes, while not identical, are sufficiently close to each other that they can be exchanged for each other in many application simulations. This probably explains why our earlier n-heptane mechanism [9] has been so useful as a diesel fuel surrogate in past studies, despite its much smaller size than conventional diesel fuel molecules; its ignition rates are close enough to those of real diesel fuels, whose ignition rate and cetane number is

established by its large n-alkane components, that diesel ignition is quite well reproduced by n-heptane.

Recent work of Dagaut et al. [44,45] has successfully used large n-alkanes as useful surrogates for kerosene and biodiesel fuels. The present work shows that the long straight-chain structure of the n-alkanes controls their ignition, and this clearly extends to long straight-chain molecules with additional functional groups attached to the end of the chain. Large n-alkanes should be successful as surrogates for other chemical species with similar structures, especially long-chain n-alkyl benzenes and n-alkyl cyclohexanes and cyclopentanes.

These mechanisms have been developed in somewhat simplified forms. We are aware of numerous improvements that would make them more general and more applicable to new systems. Perhaps most important are extensions that would make them more specific towards kinetic modeling of olefins. Other refinements should provide a more accurate theoretical description of some kinetic processes, as well as more accurate extensions to much higher pressures. Of course, mechanism upgrades and refinements add more complexity and computational costs to detailed modeling efforts. However, in the present form, these mechanisms have considerable capabilities for simulation of combustion of n-alkane fuels.

ACKNOWLEDGMENTS

This work was supported by the U.S. Department of Energy, Office of Freedom CAR and Vehicle Technologies, and the authors thank program managers Kevin Stork and Gurpreet Singh for their support of this work. This work was performed under the

auspices of the U.S. Department of Energy by the Lawrence Livermore National Laboratory under Contract DE-AC52-07NA27344.

REFERENCES

1. W. J. Pitz, N. P. Cernansky, F. L. Dryer, F. N. Egolfopoulos, J. T. Farrell, D. G. Friend, D.G., and H. Pitsch, Society of Automotive Engineers paper SAE-2007-01-0175 (2007).

2. J. T. Farrell, N. P. Cernansky, F. L. Dryer, D. G. Friend, C. A. Hergart, C.K. Law, R. M. McDavid, C. J. Mueller, A. K. Patel, and H. Pitsch, Society of Automotive Engineers paper SAE-2007-01-0201 (2007).

3. A. Violi, S. Yan, E. G. Eddings, A. Sarofim, S. Granata, T. Faravelli and E. Ranzi, Combust. Sci. Technol. 174 (2002) 399-417.

4. M. Colket, T. Edwards, S. Williams, N. P. Cernansky, D. L. Miller, F. Egolfopoulos, P. Lindstedt, K. Seshadri, F. L. Dryer, C. K. Law, D. Friend, D. B. Lenhert, H. Pitsch, A. Sarofim, M. Smooke, and W. Tsang, AIAA publication (2007).

5. W. G. Lovell, Ind. Engr. Chem. 40 (1948) 2388-2438.

6. C. K. Westbrook, W. J. Pitz, and W. R. Leppard, Society of Automotive Engineers paper SAE-912314 (1991).

7. C. K. Westbrook, W. J. Pitz, J. E. Boercker, H. J. Curran, J. F. Griffiths, C. Mohamed, and M. Ribaucour, Proc. Combust. Inst. 29 (2002) 1311-1318.

8. M. Ribaucour, R. Minetti, L. R. Sochet, H. J. Curran, W. J. Pitz, and C. K. Westbrook, Proc. Combust. Inst. 28 (2000) 1671-1678.

9. H. J. Curran, P. Gaffuri, W. J. Pitz, and C. K. Westbrook, C. K., Combust. Flame 114 (1998) 149-177.

10. H. J. Curran, P. Gaffuri, W. J. Pitz, and C. K. Westbrook, C.K., Combust. Flame 129 (2002) 253-280.

11. E. S. Blurock, J. Chem. Inf. Comp. Sci. 44 (2004) 1336-1347.

12. G. Moreac, E. S. Blurock, and F. Mauss, Combust. Sci. Technol. 178 (2006) 2025-2038.

13. G. Bikas and N. Peters, Combust. Flame 126 (2001) 1456-1475.

14. C. K. Westbrook and F. L. Dryer, Proc. Combust. Inst. 18 (1980) 749-767.

15. C. K. Westbrook, and F. L. Dryer, Prog. Energy Combust. Sci. 10 (1980) 1- 57 (1984).

16. C. K. Westbrook, and F. L. Dryer, Combust. Sci. Technol. 20 (1979) 125-140.

17. C. K. Westbrook, and W. J. Pitz, Combust. Sci. Technol. 37 (1984) 117-152.

18. W. J. Pitz, C. K. Westbrook, W. M. Proscia, and F. L. Dryer, Proc. Combust. Inst. 20 (1984) 831-843.

19. J. Li, Z. W. Zhao, A. Kazakov, M. Chaos, F. L. Dryer, and J. J. Scire, Int. J. Chem. Kinet. 39 (2007) 109-136.

20. J. Li, Z. W. Zhao, A. Kazakov, and F. L. Dryer, Int. J. Chem. Kinet. 36 (2004) 566-575.

21. M. O'Conaire, H. J. Curran, J. M. Simmie, W. J. Pitz, and C. K. Westbrook, Int. J. Chem. Kinet. 36 (2004) 603-622.

22. T. J. Held and F. L. Dryer, Int. J. Chem. Kinet. 30, (1998) 805-830.

23. S. Hochgreb and F.L. Dryer, Combust. Flame 91 (1992) 257-284.

24. E. Ranzi, A. Sogaro, P. Gaffuri, G. Pennati, C. K. Westbrook, and W. J. Pitz, Combust. Flame 99 (1994) 201-211.

25. C. Chevalier, E.J. Pitz, J. Warnatz, C. K. Westbrook, and H. Melenk, Proc. Combust. Inst. 24 (1992) 93-101.

26. Y. Muharam, and J. Warnatz, Phys. Chem. Chem. Phys. (2007) 4218-4229.

27. F. Battin-Leclerc, R. Fournet, P. A. Glaude, B. Judenherc, V. Warth, G. M. Come, and G. Scacchi, Proc. Combust. Inst. 28 (2000) 1597-1605.

28. V. Warth, N. Stef, P. A. Glaude, F. Battin-Leclerc, G. Scacchi, and G. M. Come, Combust. Flame 114 (1998) 81-102.

29. V. Warth, F. Battin-Leclerc, R. Fournet, P. A. Glaude, G. M. Come, and G. Scacchi, Comput. Chem. 24 (2000) 541-560.

30. P. A. Glaude, V. Warth, R. Fournet, F. Battin-Leclerc, G. Schacchi and G.M. Come, Int. J. Chem. Kinet. 30 (1998) 949-959.

31. R. Fournet, F. Battin-Leclert, P. A. Glaude, B. Judenherc, V. Warth,G. M. Come, G. Scacchi, A. Ristori, G. Pengloan, P. Dagaut, and M. Cathonnet, Int. J. Chem. Kinet. 33 (2001) 574-586.

32. G. Dayma, P. A. Glaude, R. Fournet, and F. Battin-Leclerc, Int. J. Chem. Kinet. 35 (2003) 273-285.

33. F. Buda, B. Heyberger, R. Fournet, P.-A. Glaude, V. Warth, and F. Battin-Leclerc, Ener. Fuels 20 (2006) 1450-1459.

34. S. Touchard, R. Fournet, P. A. Glaude, V. Warth, F. Battin-Leclerc, G. Vanhove, M. Ribaucour, and R. Minetti, Proc. Combust. Inst. 30 (2005) 1073.

35. S. Touchard, F. Buda, G. Dayma, P. A. Glaude, R. Fournet, and F. Battin-Leclerc, Int. J. Chem. Kinet. 37 (2005) 451-463.

36. G. Vanhove, R. Minetti, S. Touchard, R. Fournet, P.A. Glaude, and F. Battin-Leclerc, Combust. Flame 145 (2006) 272-281.

37. R. Bounaceur, P. A. Glaude, R. Fournet, F. Battin-Leclerc, S. Jay, and A. Pires da Cruz, Int. J. Vehicle Design 44 (2007) 124-142.

38. A. Ristori, P. Dagaut, and M. Cathonnet, Combust. Flame 125 (2001) 1128-1137.

39. C. Bales-Gueret, M. Cathonnet, J.-C. Boettner, and F. Gaillard, Energy and Fuels 6 (1992) 189-194.

40. P. Dagaut, M. Reuillon, J.-C. Boettner, and M. Cathonnet, Proc. Combust. Inst. 25 (1994) 919-926.

41. P. Dagaut, M. Reuillon, and M. Cathonnet, Combust. Sci. Technol. 103 (1994) 349-359.

42. P. Dagaut, P., Phys. Chem. Chem. Phys. 4 (2002) 2079-2094.

43. P. Dagaut, A. El Bakali, and A. Ristori, Fuel 85 (2006) 944-956.

44. P. Dagaut and S. Gail, J. Phys. Chem. A 111 (2007) 3992-4000.

45. P. Dagaut, S. Gail, and M. Sahasrabudhe, Proc. Combust. Inst. 31 (2007) 2955-2961.

46. M. Nehse, J. Warnatz, and C. Chevalier, Proc. Combust. Inst. 26 (1996) 773-780.

47. E. Olchanski and A. Burcat, Int. J. Chem. Kinet. 38 (2006) 703-713.

48. Z. Zhao, J. Li, A. Kazakov, and F. L. Dryer, Combust. Sci. Technol. 177 (2005) 89-106.

49. S. P. Zeppieri, S. D. Klotz, and F. L. Dryer, Proc. Combust. Inst. 28 (2000) 1587-1595.

50. T. J. Held, A. J. Marchese, and F. L. Dryer, Combust. Sci. Technol. 123 (1997) 107-146.

51. O. Herbinet, P.-M. Marquaire, F. Battin-Leclerc, and R. Fournet, J. Anal. Appl. Pyrolysis 78 (2007) 419-429.

52. K. D. Dahm, P. S. Virk, R. Bounaceur, F. Battin-Leclerc, P. M. Marquaire, R. Fournet, E. Daniau, and M. Bouchez, J. Anal. Appl. Pyrolysis 71 (2004) 865-881.

53. R. P. Lindstedt and L. Q. Maurice, Combust. Sci. Technol. 107 (1995) 317-353.

54. R. P. Lindstedt and L. Q. Maurice, J. Prop. Power 16 (2000) 187-195.

55. P. Dagaut and M. Cathonnet, Prog. Energy Combust. Sci. 32 (2006) 48-92.

56. F. Buda, R. Bounaceur, V. Warth, P. A. Glaude, R. Fournet, and F. Battin-Leclerc, Combust. Flame 142 (2005) 170-186.

57. E. Ranzi, A. Frassoldati, S. Granata, and T. Faravelli, Ind. Eng. Chem. Res. 44 (2005) 5170-5183.

58. F. Battin-Leclerc, Prog. Energy Combust. Sci., in press (2008).

59. N. Cohen and K. R. Westberg, Int. J. Chem. Kinet. 18 (1986) 99-140.

60. N. Cohen, Int. J. Chem. Kinet. 23 (1991) 683-700.

61. E.R. Ritter, J. W. Bozzelli, Int. J. Chem. Kinet. 23 (1991) 767-778.

62. J. Yu, R. Sumathi, and W. H. Green, J. Amer. Chem. Soc. 126 (2004) 12685-12700.

63. H. J. Curran, Int. J. Chem. Kinet. 38 (2006) 250-275.

64. D. L. Allara and R. Shaw, J. Phys. Chem. Ref. Data 9 (1980) 523-559.

65. H. Sun and J. W. Bozzelli, J. Phys. Chem. A 108 (10) (2004) 1694-1711.

66. C. Y. Sheng, J. W. Bozzelli, A. M. Dean, and A. Y. Chang, J. Phys. Chem. A 106 (2002) 7276-7293.

67. J. D. DeSain, S. J. Klippenstein, J. A. Miller, and C. A. Taatjes, J. Phys. Chem. A 107 (2003) 4415-4427.

68. H. Carstensen, C. V. Naik, and A. M. Dean, J. Phys. Chem. A 109 (2005) 2264-2281.

69. E.J. Silke, W.J. Pitz, C.K. Westbrook, M. Ribaucour, J. Phys. Chem. A. 111 (19) (2007) 3761-3775.

70. W. J. Pitz, C. V. Naik, T. N. Mhaolduin, C. K. Westbrook, H. J. Curran, J. P. Orme, and J. M. Simmie, Proc. Combust. Inst. 31 (2007) 267-275.

71. J. Bozzelli and W. J. Pitz, Proc. Combust. Inst. 25 (1994) 783-791.

72. J. Bozzelli and E. R. Ritter, E.R., *Chemical and Physical Processes in Combustion*, The Combustion Institute, Pittsburgh, 103:459 (1993).

73. G. Vanhove, M. Ribaucour, and R. Minetti, Proc. Combust. Inst. 30 (2005) 1065-1072.

74. M. Mehl and W. J. Pitz, unpublished, 2007.

75. R. T. Pollard, *Comprehensive Chemical Kinetics, Vol. 17*, (C.H. Bamford and C.F.H. Tipper, Eds.), Elsevier, New York, 1977, p. 249.

76. W. Tsang and R. F. Hampson, J. Phys. Chem. Ref. Data 15 (1986) 1087 - 1279.

77. K. A. Sahetchian, R. Rigny, J. T. De Maleissye, L. Batt, M. Anwar Khan, and S. Mathews, Proc. Combust. Inst. 24 (1992) 637-643.

78. J. C. Rienstra-Kiracofe, W. D. Allen, and H. F. Schaefer, J. Phys. Chem. A 104 (2000) 9823-9840.

79. E. L. Petersen, D. M. Kalitan, S. Simmons, G. Bourque, H. J. Curran, and J. M. Simmie, Proc. Combust. Inst. 31 (2007) 447-454.

80. D. F. Davidson, J. T. Herbon, D. C. Horning, and R. K. Hanson, Int. J. Chem. Kinet. 33 (2001) 775-783.

81. D. C. Horning, D. F. Davidson, and R. K. Hanson, J. Propul. Power 18 (2002) 363-371.

82. V. P. Zhukov, V. A. Sechenov, and A. Y. Starikovskii, Combust. Flame, in press (2008).

83. V. P. Zhukov, D. L. Tsyganov, V. A. Sechenov, and A. Y. Starikovskii, Proceedings of the European Combustion Meeting, Belgium, April 2005.

84. H. K. Ciezki and G. Adomeit, G., Combust. Flame 93 (1993) 421-433.

85. U. Pfahl, K. Fieweger, and G. Adomeit, Proc. Combust. Inst. 26 (1996) 781-789.

86. K. Kumar, G. Mittal, and C. J. Sung, Paper D05, Fifth US Combustion Meeting, March 25-28, 2007.

87. J. E. Dec, Society of Automotive Engineers publication SAE-970873 (1997).

88. E. L. Petersen, M. Lamnaouer, J. de Vries, H. Curran, J. Simmie, M. Fikri, C. Schulz, and G. Bourque, Proc. Int. Symp. Shock Waves, July, 2007.

89. S. M. Gallagher, H. J. Curran, W. K. Metcalfe, D. Healy, and J. M. Simmie, "A Rapid Compression Machine Study of the Oxidation of Propane in the Negative Temperature Coefficient Regime", Combust. Flame, in press (2008).

90. A. Cox, J. F. Griffiths, C. Mohamed, H. J. Curran, W. J. Pitz, and C. K. Westbrook, Proc. Combust. Inst. 26 (1996) 2685-2692.

91. O. Herbinet, W.J. Pitz, and C.K. Westbrook, Combust. Flame, submitted (2008).

92. A. Agosta, N. P. Cernansky, D. L. Miller, T. Faravelli, and E. Ranzi, Exper. Therm. Fluid Sci. 28 (2004) 701-708.

93. P. Zhou, O. L. Hollis, and B. L. Crynes, Ind. Eng. Chem. Res. 26 (1987) 846-852.

FIGURE CAPTIONS

Fig. 1. Overall reaction path diagram describing hydrocarbon ignition at high and low temperatures.

Fig. 2. Computed and experimental [47] ignition delay times for n-decane/O_2/Ar mixtures behind reflected shock waves. Experiments are shown as filled symbols, computed results as open symbols, so each shock is represented by a pair of symbols.

Fig. 3. Experimental [80] and computed OH mole fractions in n-decane ignition. To=1525K, ϕ = 1, n-$C_{10}H_{22}$ initial concentration is 300 ppm.

Fig. 4. Computed OH concentrations for (left) To=1706K, 300 ppm n-decane, ϕ = 1.2, and (right) To=1404K, 2000 ppm, ϕ = 1.0. Experiments from [80].

Fig. 5. Shock tube ignition delay times for n-heptane and n-decane, all at 13.5 bar pressure and stoichiometric fuel/air. Experiments are from (♦)Ciezki and Adomeit [84] and (▲) Pfahl et al. [85]. N-heptane (■) computed results from ref [9], n-decane (●) results computed from the current mechanism.

Fig. 6. Computed ignition delay times for stoichiometric n-alkanes in air at 13.5 bar.

Fig. 7. Computed temperatures during ignition of stoichiometric n-alkane/air mixtures from n-octane to n-hexadecane, showing two-stage ignitions. For each fuel, the initial temperatures are 810K and 13.5 bar pressure.

Fig. 8. Consumption of fuel during the first ignition stage for n-alkane fuels. Initial temperature in each case is 810K, 13.5 bar pressure, at stoichiometric conditions in air.

Figure 9. Computed total alkyl radical concentrations following first stage ignition for a series of n-alkanes.

Fig. 10. Computed pressures in RCM experiments at 14.3 bar pressure, ϕ = 0.8, with n-decane and air, at different compressed gas temperatures

Fig. 11. Ignition delay times at different compressed gas temperatures for n-decane/air in the RCM at ϕ = 0.8 and 14.3 bar pressure. Dashed curve, experiments [86], dotted curve, computed results [13], solid curve, present model.

Fig. 12. Ignition delay times for stoichiometric n-decane in shock tubes and rapid compression machines at approximately 14 bar pressure. RCM data (□) of Kumar et al. [86] and RCM results computed by Bikas and Peters (○)are scaled from ϕ=0.8 for comparison, RCM results computed by present model (Δ). All other symbols for shock tube ignition are the same as in Fig. 5.

Fig. 13. Computed and experimental ignition delay times for $\phi = 1$, n-decane/air at 13 atm pressure. Experiments (◊) from Zhukov et al. [82,83], present model (♦).

Fig. 14. Computed and experimental ignition delay times for $\phi = 0.5$, n-decane/air at 80 atm pressure. Experiments (◊) from Zhukov et al. [82,83], present model (♦).

Fig. 15. Computed and experimental ignition delay times for $\phi = 1.0$, n-decane/air at 80 atm pressure. Experiments (◊) from Zhukov et al. [82,83], present model (♦).

Fig. 16. Ignition delay times for stoichiometric n-decane in shock tubes and rapid compression machines at approximately 14 bar pressure. Experimental high temperature shock tube results from Zhukov et al. [82,83] shown by (◊), present model by (Δ). All other symbols are the same as in Fig. 12.

Fig. 17. Comparisons of shock tube experimental and computed ignition delay times of Zhukov et al. [82,83] at 80 bar (□)and Pfahl et al. [85] at 50 bar (◊), for n-decane at ϕ=1. Filled symbols show corresponding computed results.

Fig. 18. Fuel and major pyrolysis products of n-decane in the Princeton flow reactor [48,49], 1456 ppm n-decane, 1060K, 1 atm. Lines show computed results, symbols show experimental results. Ethene (▲, dashed line), propene (■, dotted line), n-decane (♦, solid line), ethane (●, dot-dash line)

Figure 19. Major species concentrations for n-decane oxidation, To = 1019K, 1452 ppm n-decane, $\phi = 1.0$, 1 atm. Lines show computed results, symbols show experimental results [48,49]. n-cetane (■, solid line), ethene (▲, dashed line), CO (♦, dotted line), propene (Δ, dash-dot line)

Figure 20. Intermediate species concentrations in n-decane oxidation, same conditions as Fig. 19. Lines show computed results, symbols show experimental data [48,49]. Propene (▲, solid line), methane (■, dot-dash line), 1-butene (♦, dotted line), 1-hexene (●, dashed line)

Fig. 21. Chemical species concentrations in a jet stirred reactor oxidation of n-decane, 10 atm pressure, 1000 ppm n-decane, $\phi = 1.0$, residence time of 0.5 s. Lines represent computed values, symbols are experimental results [39].

Figure 22. Computed levels of decenes produced in oxidation of n-decane in jet-stirred reactor, same conditions as in Fig. 21. Concentration of n-decane is shown for comparison.

Figure 23. Concentrations of 1-olefins produced during oxidation of n-decane in a jet-stirred reactor. Same conditions as Fig. 21.

Fig. 24. Comparison between computed and experimental [38] results for selected species in n-$C_{16}H_{34}$ oxidation in a JSR. Conditions are ϕ = 1.5, 1 atm pressure, and 0.07 s residence time.

Fig. 25. Major species profiles in JSR oxidation, comparing RME experiments [38] and present n-hexadecane model. Conditions are 1 atm, 0.07 s residence time.

Fig. 26. Fuel concentrations in jet-stirred reactor simulations. Initial values are scaled to 700 ppm in n-decane for comparison. Mixtures are stoichiometric, 10 atm pressure, residence time of 0.07 s. Experimental values are shown for n-decane (symbols) [42].

Fig. 27. Computed concentrations of ethene (solid lines), methane (dashed lines) and 1-butene (dotted lines) for n-alkane fuels under jet-stirred reactor conditions. Symbols represent experimental values from Dagaut et al. [42] for n-decane oxidation, ethene (□), methane (◊), and 1-butene (Δ).

Fig. 28. Computed and experimental CO concentrations in pressurized flow reactor [91], at 8 atm, residence time of 120 ms. Computed values are shown for curves with filled symbols, experiments with open symbols, ϕ = 0.2 (◊ and ♦), and ϕ = 0.3 (□ and ■).

Fig. 29. Products of n-dodecane thermolysis at 893K, experiments from Zhou et al. [92] at 1 atm, . Residence time for experiments is 3.3 s, for computed results 1.0 s. Experimental results are solid bars, computed results are shaded.

Fig. 30. Products of n-nonane thermolysis at 893K, experiments from Zhou et al. [92] at 1 atm, . Residence time for experiments is 1.5 s, for computed results 0.5 s. Experimental results are solid bars, computed results are shaded.

Fig. 31. Conversion of fuel and species produced in n-dodecane pyrolysis (2% n-dodecane, 98% He) at 1 second residence time for a range of temperatures. Experimental values [51] are shown as symbols, lines show computed results, dashed curves include retroene reactions of 1-alkenes.

Fig. 32. Fuel conversion and species histories in n-dodecane pyrolysis [51] (2% n-dodecane, 98% He) . Temperature is 973K, symbols are experimental points, lines are computed results. Dashed curves include retroene 1-alkene decompositions, solid curves do not include them.